

# **INVESTIGATION ON METHODS AND MODELS FOR MATERIAL IDENTIFICATION USING SPHERICAL INDENTATION**



Nick Andreievich Contente Pires Kossolapov

14344042

Supervisor: Prof. S. Kok

Department of Mechanical and Aeronautical Engineering

Faculty of Engineering, Built Environment and Information Technology

UNIVERSITY OF PRETORIA

October 2017

## ABSTRACT

Title: Investigation on Methods and Models for Material Identification using Spherical Indentation  
Author: N.A. Kossolapov  
Student Number: 14344042  
Supervisor: Prof. S. Kok  
Year: 2017

Indentation tests are often used to determine the stress-strain curve of a material where direct measurement methods can't be used, i.e. for thin films or because the equipment of interest is in use. Typically, a heuristic method, an analytical procedure, or direct optimisation is used to solve this inverse problem. A spherical indentation test was performed to find the force versus deflection ( $F-h$ ) curve of the reaction load on the indenter. To complement the investigation, a virtual indentation test was analysed where the stress-strain curve is known beforehand. Different material models were explored. Direct minimisation was used on both the real indentation test data and the virtual data. Alternative techniques were applied to the virtual problem and compared with each other, namely a radial basis function surrogate model and partial least squares regression. With increasingly flexible material models, it was possible to match the experimental  $F-h$  curve more accurately. However, the solutions for the different models would produce non-converging results with an increase in model flexibility. This was also seen when analysing the virtual problem, as stress-strain curves were found which produced nearly identical  $F-h$  curves yet were not the best approximation of the virtual material's true stress-strain curve. Thus, a lack of uniqueness was found in the problem. Many authors reported solutions without much regard to the uniqueness of the problem. However, the results of the investigation show that the uniqueness of the problem should be placed under more scrutiny.

## **ACKNOWLEDGEMENTS**

I would like to acknowledge and extend my sincere gratitude to the people who assisted with my project, often out of their own time.

Prof. Schalk Kok, my supervisor, for all his guidance, advice, and assistance throughout this research project.

Prof. Pieter Pistorius, for all his technical advice and assistance with getting the test samples scanned.

Mr Peet Kruger, for manufacturing parts for me and for assisting in preparing test samples, and Mr Herman Booyens, for his assistance with the experiment.

## TABLE OF CONTENTS

I.	Introduction.....	1
II.	Background .....	2
A.	Literature Survey .....	2
1.	Indentation Test for Obtaining Material Parameters .....	2
2.	Geometry.....	2
3.	FEM Model Setup.....	2
B.	Ill-posed Problems .....	3
C.	Plasticity .....	3
1.	Yielding.....	3
2.	Yield Surface .....	4
3.	Strain-Hardening.....	4
4.	Hardening Rules.....	5
D.	Stress-Strain Relationships.....	5
III.	Experiment .....	7
A.	Experimental Setup.....	7
B.	Experimental Results.....	8
IV.	Numerical Setup.....	10
A.	Software Packages .....	10
B.	Finite Element Model .....	10
1.	Geometry.....	10
2.	Mesh.....	11
3.	Static Boundary Conditions .....	12
C.	Machine Compliance .....	12
D.	CalculiX Input File .....	13
1.	Contact .....	13
2.	Friction .....	14
3.	Plasticity.....	15
4.	Dynamic Boundary Conditions.....	15
E.	Numerical Techniques.....	16
1.	Direct Minimisation .....	16
2.	Database Methods .....	16
V.	Experimental Problem.....	18
A.	Exclusion of Surface Profiles .....	18

B.	One Parameter Model.....	18
1.	Analysis of One Parameter Model.....	20
C.	Evaluation Criterion for Entire Curve .....	20
D.	Higher Parameter Models.....	20
1.	Two Parameter Model.....	21
2.	Three Parameter Model.....	22
3.	Four Parameter Models.....	23
E.	Comparison of Models .....	24
F.	Comparison with Frictionless Model .....	26
G.	Effect of Indenter on F-h Curve .....	27
H.	Uniqueness of Problem.....	29
I.	Pitfalls of Experimental Data .....	30
VI.	Virtual Problem.....	31
A.	Direct Optimisation with Surface Profile .....	31
B.	Parameterisation of Problem .....	33
C.	Database Sampling .....	34
D.	Radial Basis Function Surrogate Model .....	35
1.	Presence of Family of Solutions .....	37
E.	Statistical Regression.....	39
F.	Analysis of Database Techniques.....	43
G.	Uniqueness of Problem.....	43
1.	Intermediate Surface Profiles.....	44
2.	Non-spherical Indenter.....	45
3.	Source of Lack of Uniqueness .....	47
VII.	Conclusion.....	49
	References .....	51
	Appendix A: Meeting Log Card .....	A1
	Appendix B: Research Project Proposal .....	B1
	Appendix C: Progress Reports .....	C1
	Appendix D: Calculix Input Files .....	D1
	Appendix E: Uniaxial Test Data .....	E1
	Appendix F: Database techniques .....	F1
	Appendix G: Inclusion of Surface Profile in Direct Optimisation.....	G1
	Appendix H: Plastic strain distributions .....	H1

## LIST OF FIGURES

Figure 1 Correlating F-h data to $\sigma$ - $\epsilon_p$ data.....	1
Figure 2 Hydraulic press experimental setup.....	7
Figure 3 Complete F-h curves for 40 mm aluminium samples.....	8
Figure 4 Selected F-h curves for 40 mm aluminium samples.....	9
Figure 5 Line scan surface of sample.....	9
Figure 6 Line labelling for FEM model .....	11
Figure 7 Mesh of the model .....	11
Figure 8 Indenter contact area detail .....	11
Figure 9 Element contact at axis of rotation during indentation.....	12
Figure 10 Effect of press stiffness on F-h curve .....	13
Figure 11 Shear stress versus relative tangential displacement in CalculiX.....	14
Figure 12 Effects of friction on the F-h curve.....	15
Figure 13 Ratio of friction and frictionless F-h loading curves for random $\sigma$ - $\epsilon_p$ curves ....	18
Figure 14 F-h curve for one parameter model .....	19
Figure 15 F-h curve for two parameter model .....	21
Figure 16 F-h curve for three parameter model .....	22
Figure 17 $\sigma$ - $\epsilon_p$ curves for different models .....	24
Figure 18 Models compared to bands of experimental data .....	25
Figure 19 Detail view of models compared to bands of experimental data .....	25
Figure 20 F-h curves for friction and frictionless three parameter model .....	26
Figure 21 Surface profile for frictionless three parameter model .....	27
Figure 22 FEM model of indenter and holder.....	28
Figure 23 F-h curves for different indenter models .....	28
Figure 24 Contour plot of the relative F-h MSE with fixed saturation constant.....	29
Figure 25 Stress distribution in indenter .....	30
Figure 26 Relative MSE for F-h curve.....	31
Figure 27 Relative MSE for surface profile .....	32
Figure 28 Relative MSE for $\sigma$ - $\epsilon_p$ curve.....	32
Figure 29 $\sigma$ - $\epsilon_p$ curves for mapping three parameter model to power law curve .....	33
Figure 30 F-h curves for fitting three parameter model to power law curve .....	34
Figure 31 MSE of $\sigma$ - $\epsilon_p$ curve for surrogate model estimation with uniform database .....	35
Figure 32 MSE of $\sigma$ - $\epsilon_p$ curve for surrogate model estimation with LHS database.....	36
Figure 33 $\sigma$ - $\epsilon_p$ curves for the best surrogate model estimation.....	36
Figure 34 $\sigma$ - $\epsilon_p$ and F-h curves for the mean surrogate model estimation .....	37
Figure 35 $\sigma$ - $\epsilon_p$ and F-h curves for the 95 <sup>th</sup> percentile surrogate model estimation .....	37
Figure 36 Contour plot of the MSE for the F-h curve with fixed b parameter .....	38
Figure 37 Contour plot of the MSE for the F-h curve with fixed m parameter .....	38
Figure 38 Contour plot of the MSE for the F-h curve with fixed $\sigma_0$ parameter.....	39
Figure 39 MSE of $\sigma$ - $\epsilon_p$ curve for PLS using parameters.....	40
Figure 40 MSE of $\sigma$ - $\epsilon_p$ curve for PLS using $\sigma$ - $\epsilon_p$ curves .....	40
Figure 41 $\sigma$ - $\epsilon_p$ and F-h curves for the mean PLS prediction.....	41
Figure 42 $\sigma$ - $\epsilon_p$ and F-h curves for the 95 <sup>th</sup> percentile PLS prediction.....	41
Figure 43 PLS $\sigma_0$ parameter predictions .....	42
Figure 44 PLS b parameter predictions.....	42

Figure 45 PLS m parameter predictions.....	42
Figure 46 Target and worst fit $\sigma$ - $\epsilon_p$ curves.....	44
Figure 47 Target and worst fit F-h curves with multiple unloading steps .....	45
Figure 48 Target and worst fit surface profiles with multiple unloading steps .....	45
Figure 49 Target and worst fit F-h curves with multiple unloading steps .....	46
Figure 50 Target and worst fit surface profiles with multiple unloading steps .....	46
Figure 51 Stress distribution in target material .....	48
Figure 52 Stress distribution in worst-fit material with target material stress contours .....	48

## LIST OF TABLES

Table 1 Input properties for GraphiX meshing .....	10
Table 2 Optimal one parameter model's parameters .....	19
Table 3 Optimal two parameter model's parameters.....	21
Table 4 Optimal three parameter model's parameters.....	23
Table 5 Relative minimum error of different models .....	24
Table 6 Centre for databases .....	35

## NOMENCLATURE

<i>Symbol</i>	<i>Property</i>
$E$	Young's modulus, tangent modulus
$F$	Force
$J$	Scalar invariant
$K$	Material constant
$S_y$	Proof stress
$W$	Work
$W_s$	Specific work
$X$	Independent variable matrix
$Y$	Dependent variable matrix
$b$	Saturation constant
$e$	Error
$h$	Displacement, relative height
$k$	Material constant
$n$	Strain hardening exponent
$m$	Initial work hardening rate constant
$r$	Radial distance, distance between two points
$w$	Weighting factor
$x$	Parameter or independent variable
$y$	Parameter or dependent variable
$\alpha$	Shift-stress tensor
$\varepsilon$	Strain
$\varepsilon_p$	Plastic strain
$\epsilon$	RBF shape parameter
$\theta$	Initial work hardening rate
$\lambda$	Stick slope
$\mu$	Coefficient of friction
$\sigma$	Stress
$\sigma_0$	Yield Stress
$\sigma_e$	Evolving Stress
$\sigma_s$	Saturation Stress
$\phi$	Radial basis function
$\varphi$	Data value

## I. INTRODUCTION

It often is necessary to be able to determine the material properties of certain equipment. If the equipment is in use, non-destructive methods have to be used. Once such method is using a micro-indentation test to obtain the applied force versus displacement curve of the material, the  $F$ - $h$  curve. The stress-strain curve can then be extracted from this data through inverse analysis.

However, the force versus deflection data will not yield the true stress-strain curve of a material directly, as no analytical relations exist for plastic spherical indentation. One method to obtain a stress-strain curve is to perform an inverse analysis using finite element analysis to match the results obtained by the indentation test. Typically for engineering applications the stress-strain curve of a material in a structure is known, and the forces or deflections of the structure need to be determined. Therefore, the analysis for the problem will involve the inverse of this.

In a broad sense, the analysis will involve taking data in some force-displacement domain and finding the corresponding stress – plastic strain curve as seen in Figure 1. As such, this procedure may be adapted for other structural mechanics' problems, such as determining the stress-strain curve of a material in a tensile test after necking.

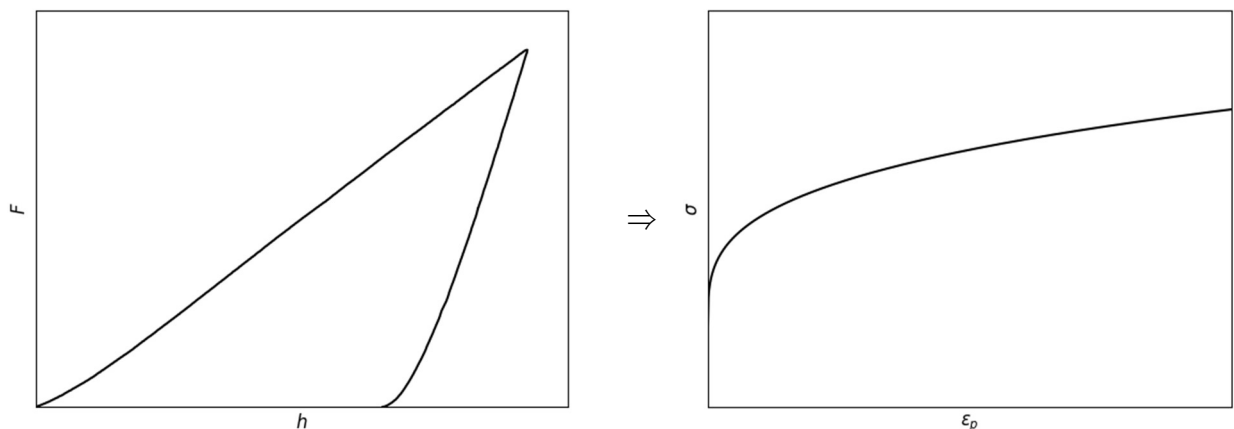


Figure 1 Correlating  $F$ - $h$  data to  $\sigma$ - $\epsilon_p$  data

Additional information may also be included in the inverse problem, such as trying to match the  $F$ - $h$  curve alongside the surface profile of the indentation. This will require using the height versus radial distance of the indentation, or the  $r$ - $h$  data.

This project is thereby concerned with developing this procedure. This includes exploring different techniques for the procedure. The 3 main goals originally associated with this project are:

- To plan, setup, and perform an indentation test.
- To simulate the problem using finite element software.
- To obtain the stress-strain curve of the material using data from the finite element simulations.

To these ends, the problem addressed in this project is the inverse problem of identifying the stress-strain curve of aluminium using an indentation test.

## II. BACKGROUND

Obtaining material properties using spherical indentation is not a new or novel technique, and work has been done on it. This chapter gives a brief description of literature read as well as a basic theoretical overview on the problem.

### A. Literature Survey

#### 1. Indentation Test for Obtaining Material Parameters

Using an indentation test to obtain material properties was notably first explored in 1951 by Tabor (1951). In his book, Tabor presented a correlation between the plastic strain in an indentation test,  $\varepsilon_p$ , and the indentation geometry. Other authors have worked on this basis and developed relationships between the indentation geometry and other various mechanical properties.

Inverse method techniques have also been developed for this problem. Gelin & Ghouti (1996) have developed a general inverse solution for this problem. They also found that for large plastic deformations the use of an inverse method can be more accurate than direct identification methods normally used, such as a uniaxial tensile test. Other areas of sciences have also found application in obtaining material parameters such as Bayesian inference or neural networks, explored by Wang, et al. (2016) and Tyulyukovskiy & Huber (2006) respectively.

Mackerle (2001) compiled a bibliography from 1997 to 2000 alone of finite element simulations of indentation problems, many of which involve obtaining material properties from indentation tests, again attesting to the technique's use.

#### 2. Geometry

It has been shown by Norbury & Samuel (1928) that the final indentation geometry is dependent on the material. Notably, that the crater of the indentation experiences pile-up or sinking in for low strain-hardening or high strain-hardening materials respectively.

However, Beghini, et al. (2006) found that there is no direct correlation between crater shape and the indentation properties. This could indicate that while geometry of the indentation is dependent on material properties, it is not a unique relationship.

#### 3. FEM Model Setup

The experiment used a spherical indenter, and Beghini, et al. (2006) states that while sharp indenters are often modelled as rigid bodies, a spherical indenter cannot be modelled as such. They found that it is suitable to model the indenter as a purely elastic indenter.

For the influence of friction on the  $F$ - $h$  curve, Taljat, et al. (1998) and Laursen & Simo (1992) found that above a certain friction coefficient, any changes in the coefficient produces negligible effects on the  $F$ - $h$  curve. However, it was found in both cases that differences in friction will influence the stress distribution beneath the indenter.

For the specific values for friction, Taljat et al. found the limit for the friction coefficient to be 0.2, with frictionless or low friction coefficients producing large differences in computed data. In contrast, Laursen & Simo found that a frictionless model was sufficiently accurate, imposing only contact penalties in their simulations.

## **B. Ill-posed Problems**

A well-posed problem is defined in a mathematical sense by Hadamard (1902) as a problem in which:

1. A solution exists.
2. The solution is unique.
3. The solution's behaviour changes continuously with initial conditions.

An ill-posed problem is therefore a problem in which any of these conditions are not true. A pure problem may be well-posed, but still highly sensitive to initial conditions and numerical instabilities. In such instances the problem is called ill-conditioned. Inverse problems are often ill-posed.

However, for engineering applications these definitions are unwieldy. In any physical system a degree of error will be present, and if the problem is sufficiently sensitive to initial conditions many solutions may be found to solve the problem within error. As such, the practical solution is not unique within the limits of equipment accuracy. But based on this definition, a problem being ill-posed is a spectrum of how insensitive it is to initial conditions. In the event that a problem is ill-posed in an engineering sense, additional information about the problem is needed to distinguish between true and false solutions.

As such, a non-unique solution is referred to in this report in an engineering sense as solutions which are within experimental error, resulting in an ill-posed problem.

An investigation on the uniqueness of the problem of material identification using an indentation test was often not found in literature, particularly with spherical indentation. Kang, et al. (2011) suggested that multiple indenters should be used in order to bring uniqueness into the problem. Conversely, Chen, et al. (2007) brought up the issue of uniqueness in materials, even when using techniques commonly used to impose uniqueness to a problem, such as multiple indenters.

## **C. Plasticity**

The plastic deformation of a material is when the material under application of a load deforms in a non-reversible manner. However, during plastic deformation, elastic deformation is still present, and as such the strain can be broken up into elastic and plastic components, given by

$$\varepsilon_{total} = \varepsilon_{elastic} + \varepsilon_{plastic}. \quad (2.1)$$

The elastic strain can be computed given a stress state in a material. Currently only empirical relationships are able to characterise the plastic strain component.

### **I. Yielding**

To mark onset of plastic deformation, a critical stress is reached in the material, known as the yield stress. The plastic stress-strain transition region, where the dominant deformation in the system changes from elastic to plastic, will occur around this critical stress.

Many materials do not exhibit a distinct point where this transition occurs, such as aluminium. In order to parameterise the material, an arbitrary point is chosen to define the yield stress. A common point is the offset yield point, or proof stress, where the yield point is defined where 0.2% plastic strain has occurred. Proof stress for 0.2% plastic strain is indicated by  $S_{y,0.2}$ .

## 2. Yield Surface

Yield in a material is a function of the stress state, and so it will take the form

$$F(\sigma_{11}, \sigma_{22}, \sigma_{33}, \sigma_{12}, \sigma_{23}, \sigma_{31}) = k. \quad (2.2)$$

Here  $k$  is some constant which will depend on the material, and may vary as the stress state changes. As the stress components are dependent on orientation of the axes, it is more convenient to express the yield function as

$$F(\sigma_1, \sigma_2, \sigma_3) = k, \quad (2.3)$$

where  $\sigma_1, \sigma_2, \sigma_3$  are the principal stresses. It should be noted that this equation is only valid for isotropic materials, as otherwise an additional parameter  $\mathbf{n}_i$ , the orientation of the principal directions relative to the material directions, is needed. As the yield surface is a function of three independent parameters, the function  $F$  will take the form of a surface of some shape in the  $\sigma_1\text{-}\sigma_2\text{-}\sigma_3$  domain.

A well-known example of a yield surface would be the Von Mises criterion,

$$F(\sigma_1, \sigma_2, \sigma_3) = \frac{1}{\sqrt{2}} \sqrt{(\sigma_1 - \sigma_2)^2 + (\sigma_2 - \sigma_3)^2 + (\sigma_3 - \sigma_1)^2} = \sigma_0. \quad (2.4)$$

It is possible to describe this relationship in terms of principal scalar invariants. In which case the Von Mises criterion is used in  $J_2$  plastic flow theory in the form

$$f(J_2) \equiv J_2 - k^2 = 0. \quad (2.5)$$

It has been found through experimental data that ductile materials follow this yield surface sufficiently (Downling, 1999). However, it has been shown by Gao, et al. (2009) that the Von Mises criteria (the second scalar invariant) is insufficient for the ductile failure of aluminium, which will require including the Lode angle in the model in the form of another scalar invariant. The indentation tests in this research project will not reach loads where failure occurs, and so these additional scalar invariants will not be needed.

## 3. Strain-Hardening

In a perfectly-plastic material, Chakrabarty (2006) gives the initial yield surface, as well as subsequent yield surfaces, in the form

$$f_0(\sigma_{ij}) = 0. \quad (2.6)$$

However, in a non-perfectly plastic material, the yield surface may change in shape, size, and position. These changes in the yield surface can be given in the form

$$f(\sigma_{ij}, K_i) = 0. \quad (2.7)$$

$K$  represents some hardening parameters. These parameters will describe how the yield surface changes during plastic deformation. In order to fully capture any change in the yield surface, the parameters may be scalars or higher order tensors. Indirectly, these parameters are obtained in this research project.

#### 4. Hardening Rules

In order to model the hardening parameters, some common hardening rules are typically used, namely isotropic hardening, kinematic hardening, or mixed hardening. There are more complex hardening rules which can be used, i.e. to describe complex and anisotropic shape changes, but these will not be discussed. The hardening given here are those as described by Chakrabarty (2006).

*Isotropic Hardening* – isotropic hardening will take the form

$$f(\sigma_{ij}, K_i) = f_0(\sigma_{ij}) - K = 0. \quad (2.8)$$

This produces a yield surface which maintains its shape while changing its scale. This means that the yield surface will expand with an increasing stress. By extension, this also means that the origin of the yield surface will not move.

*Kinematic Hardening* – in contrast to isotropic hardening, kinematic hardening allows the translation of the yield surface. This allows the hardening rule to model cyclic loads and the Bauschinger effect. For the case where the yield surface does not change shape or size, the yield function takes the form

$$f(\sigma_{ij}, K_i) = f_0(\sigma_{ij} - \alpha_{ij}) = 0. \quad (2.9)$$

Here the hardening parameter is  $\alpha$ , also known as the shift-stress tensor, which will characterise how the origin of the yield surface changes given a stress state.

*Mixed hardening* – both isotropic and kinematic hardening can be combined to create a mixed hardening rule. The increased complexity of the rule allows it to be a more accurate representation of reality, however this rise in complexity means the hardening parameters will be more difficult to model.

Mixed hardening can take the form

$$f(\sigma_{ij}, K_i) = f_0(\sigma_{ij} - \alpha_{ij}) - K = 0. \quad (2.10)$$

#### D. Stress-Strain Relationships

In order to characterise work hardening, relationships between the stress and strain in plastic flow need to be parameterised. Many existing models include a strain-hardening exponent,  $n$ , Young's modulus,  $E$ , and a proportionality limit stress. Also contained in these models are other material constants which are found by curve-fitting the model to a known stress-strain curve (often obtained from uniaxial tests).

One commonly used relationship is the Ramberg-Osgood model of plasticity, which is given as

$$\varepsilon = \frac{\sigma}{E} + \left(\frac{\sigma}{b}\right)^n. \quad (2.11)$$

Here  $b$  represents some material constant. The relationship can also be piecewise, such as Holloman's power law. The law is given as

$$\sigma(\varepsilon) = \begin{cases} E\varepsilon, & \varepsilon \leq \frac{\sigma_0}{E} \\ K\varepsilon^n, & \varepsilon > \frac{\sigma_0}{E} \end{cases}. \quad (2.12)$$

Here, a different material constant  $K$  is present, commonly known as the strength coefficient.

In the software package used, *CalculiX*, the solver computes plasticity in a piecewise manner, such that the final stress-strain curve used in the program is the combination of elastic and plastic strains as in equation (2.1), given by

$$\varepsilon(\sigma) = \begin{cases} \frac{\sigma}{E}, & \sigma < \sigma_0 \\ \frac{\sigma}{E} + \varepsilon_p(\sigma), & \sigma \geq \sigma_0 \end{cases}. \quad (2.13)$$

A variety of models were explored in this research project to characterise the plastic strain relationship, the  $\sigma$ - $\varepsilon_p$  curve, ranging from a simple one parameter model to four parameter models.

### III. EXPERIMENT

This chapter gives an overview of the experimental setup used for this project. Due to the primarily numerical nature of the project, the practical experiment was composed of a simple indentation test. In literature, the indentation was typically with micro-indentation. To simplify the procedure, a macro-indentation test was done instead.

Indentation tests are usually used to determine a material's hardness, i.e. only measuring the final state of the indentation. For the experiment, continuous readings of the entire  $F$ - $h$  curve of the indentation had to be captured.

#### A. *Experimental Setup*

The indentation test was performed at the University of Pretoria's Sasol Labs. A Schenck 100 kN hydraulic actuator with a LCS 100 kN load cell was used. The hydraulic actuator had its own internal LDT to measure displacement. A custom made indenter holder was manufactured from En24 steel. The experimental setup can be seen in Figure 2.



*Figure 2 Hydraulic press experimental setup*

A 40 mm diameter 6082-T6 Aluminium alloy cylindrical extrusion obtained from Non Ferrous Metal Works Pretoria was used. The material was parted into 24 mm long samples, both ends of the sample were faced, and one side was sanded, roughly polished, and cleaned to produce a smooth dirt-free surface. A standard 10 mm diameter steel ball bearing was used as an indenter. The grade of steel used in the ball bearing is not known, and so typical mechanical properties for hardened steel were assumed for the indenter.

## B. Experimental Results

This section outlines the raw experimental data obtained, namely the  $F$ - $h$  curve and the surface profile. Both sets of data would need to be interpolated for numerical analysis. To facilitate this, the data sets were smoothed with a Savitzky–Golay filter (Savitzky & Golay, 1964).

The results of all the indentations can be seen in Figure 3. Also included in the figure is the average of all the tests. The loading curve is the portion of the curve that extends from 0 mm to approximately 1.4 mm. The unloading curve is the portion of the curve from the peak of the curve to approximately 1 mm.

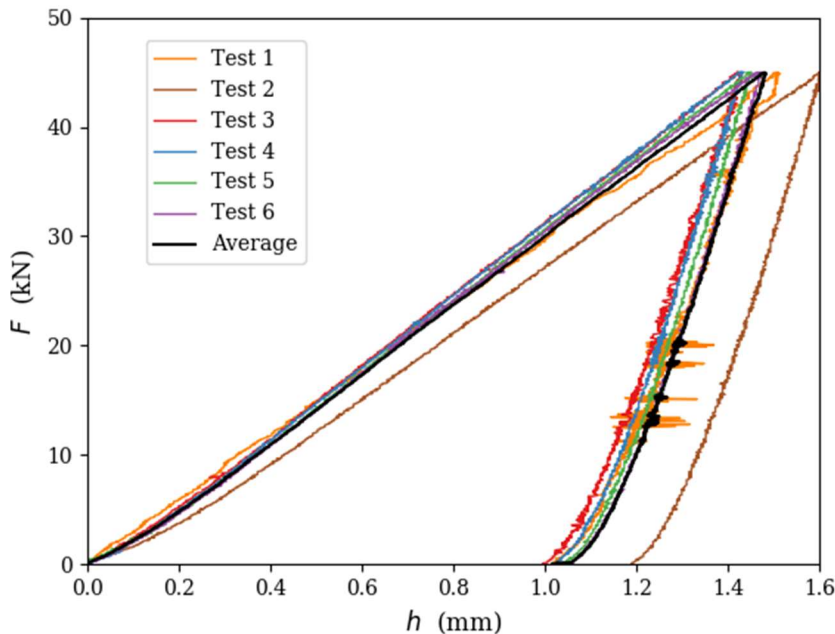


**Figure 3** Complete  $F$ - $h$  curves for 40 mm aluminium samples

Several observations can be taken from the data. The first test has very erratic behaviour, particularly during the unloading curve. The source of the noise is unknown. It is possible that the hydraulic press was not able to smoothly deliver the load as it was still warming up.

Test 2 appears to be a statistical outlier. It is approximately 20% greater in displacement than the other tests. However, it appears to be a scaled version of the other tests.

If test 1 and 2 are discarded, the resultant data can be seen in Figure 4. The spread of the curves is much closer, in particular the loading curve. The average between these curves was filtered to produce a smooth curve without distorting the shape, and was used in the numerical analysis as the target curve to be matched.

A sample was scanned by CSIR’s National Laser Centre using a 2950-25/BL Laser Line Scanner from Micron Epsilon. The line scan produces height versus radial distance data of the indentation, producing the surface profile as seen in Figure 4. This data is used to compare the output of the FEM to ensure that not only is the  $F$ - $h$  curve being satisfied, but so is the final geometry of the indentation. Relative to the original surface height of the sample, the indentation had a depth of 1.08 mm and a diameter of 6.56 mm, as shown by the green and red lines respectively on Figure 5.

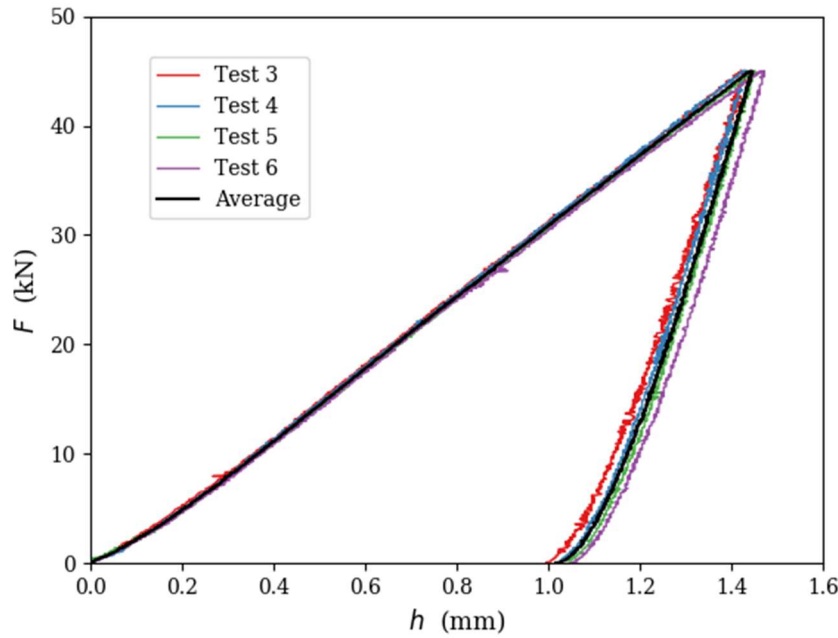


**Figure 4** Selected  $F$ - $h$  curves for 40 mm aluminium samples

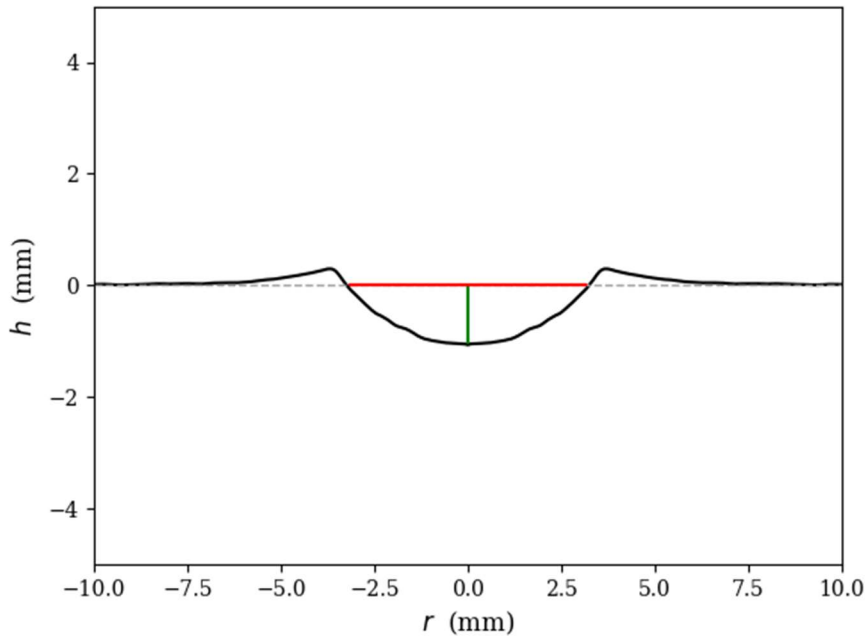


**Figure 5** Line scan surface of sample

Several samples were used in both uniaxial tensile and compressive tests in order to obtain the true plastic curves. Samples of the experimental data are shown in Appendix E. Due to machine error, there were large variances in the compression data as seen in Figure E1, or major irregularities in the tensile data as seen in Figure E2, and so the data cannot be used.

However, both tests indicate that the yield stress of the aluminium tested is above the 250 MPa value given by the manufacturer, as a minimum yield stress of 280 MPa was obtained between all data sets.

## IV. NUMERICAL SETUP

This section outlines the software environment used to model and simulate the indentation test, and how this environment was setup.

### A. Software Packages

The finite element package used was bConverge's *CalculiX for Windows* 2.10 running on an Intel i5-7600k. Python and its libraries were used for any programming requirements. Meshing was done using *GraphiX* (*CalculiX*'s graphical suite), using the built-in meshing capabilities.

An adaptive environment was programmed to facilitate running, processing and storing the data of multiple simulations with varying inputs for optimisation or database building. The simulation environment can be found online at [www.github.com/nickkossolapov/mrn](https://www.github.com/nickkossolapov/mrn).

### B. Finite Element Model

An axisymmetric model was used in order to greatly reduce computation time. Appendix D contains the template for the *CalculiX* input file and the *GraphiX* script used to generate the finite element model. The model uses the *N-mm-MPa* consistent set of units.

#### 1. Geometry

Using *GraphiX*, the perimeters of the rotational cross-section of the indenter and the sample were drawn, as seen in Figure 6. Points were added along these lines, with bias to concentrate the elements around the indentation zone.

The bias used in *GraphiX* is to specify the ratio of the largest and smallest element sizes on a line, and then adjusts all the element's sizes on a line to fit with linearly changing side lengths. Table 1 provides the properties used in the FEM model, which matched the dimensions of the sample used in the experiment.

A single layer of elements was added between L004 and L005 to provide for the machine compliance as per section IV.C.

*Table 1 Input properties for GraphiX meshing*

	Input Length	Points	Bias
l1	5	40	1.05
l2	5	20	1
peri	-	60	1.05
L001, L002	24	40	64
L003, L004, L005	20	120	32
L006, L007	5	2	1

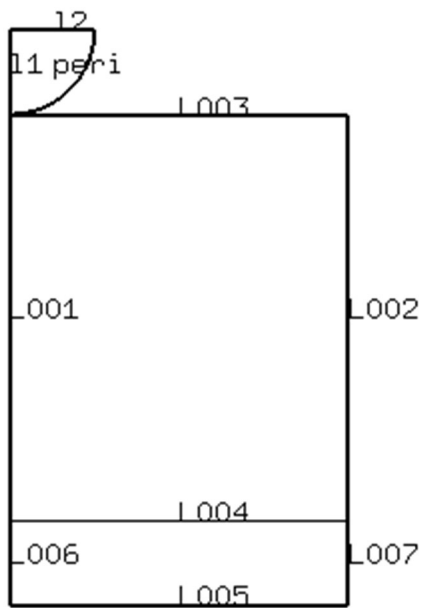


**Figure 6** Line labelling for FEM model

## 2. Mesh

The overall mesh can be seen in Figure 7, with a detail view of the indenter contact area in Figure 8.

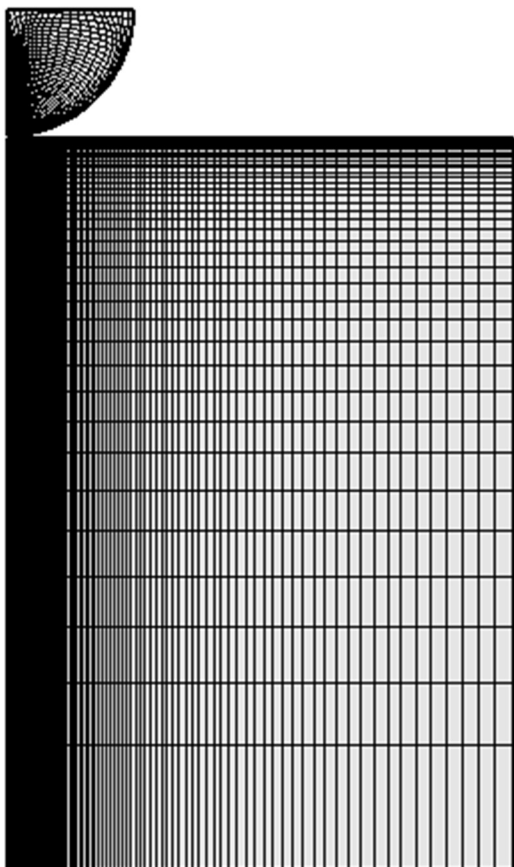


**Figure 7** Mesh of the model

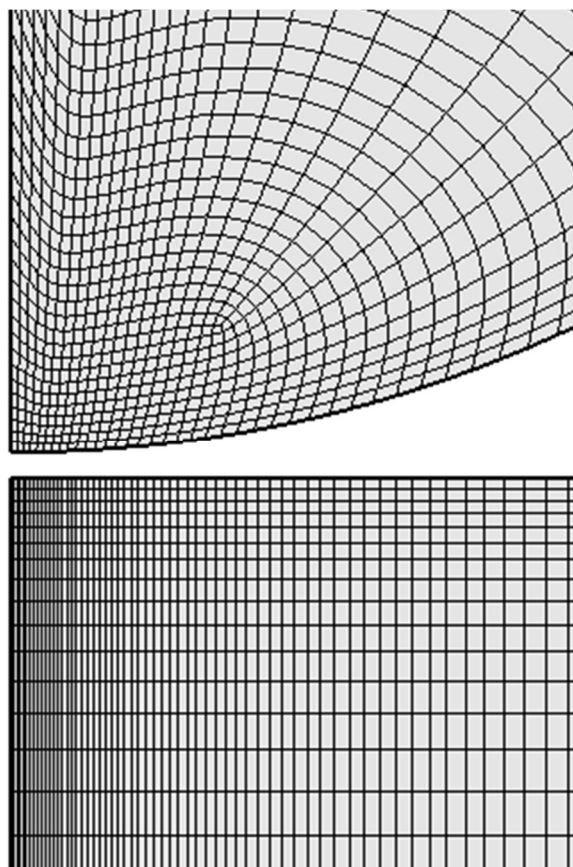


**Figure 8** Indenter contact area detail

The indenter was raised 0.1 mm above the surface of the block. This was done to allow for a few simulation steps before contact was made such that contact could be resolved without issue.

The mesh was generated using 4-node axisymmetric elements, CAX4 in *CalculiX*. 4-node elements are known to be prone to shear and volumetric locking compared to quadratic elements. Despite this, the 4-node elements allowed for faster convergence times and a reduction of stick-and-slip effects at the contact interface without notably influencing the data.

*CalculiX* does not implement true axisymmetric elements. Rather, it sweeps the 2D mesh two degrees, and then applies the appropriate boundary conditions and solves the 3D problem, mimicking a true axisymmetric element (Dhondt, 2016). This has the negative effect of causing instabilities and contact errors near the axis of rotation as seen in Figure 9. At the axis of rotation with the contacting swept element, two nodes will be placed at the same location which in turn causes issues with regards to contact. Due to the small number and size of affected elements, it would not severely influence the overall *F-h* curve.

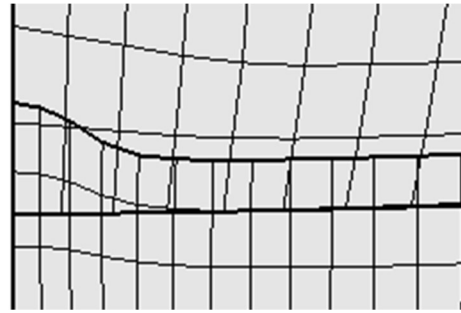


**Figure 9** Element contact at axis of rotation during indentation

### 3. Static Boundary Conditions

Due to the axisymmetric nature of the problem, certain boundary conditions had to be imposed. Lines L11, L001, and L006 were constrained horizontally, and the bottom of the sample L005 was constrained vertically. This was deemed adequate as many authors used similar boundary conditions with axisymmetric models.

### C. Machine Compliance

The initial gradient of the unloading section,

$$\frac{1}{S} = \left. \frac{dF}{dh} \right|_{h=h_{max}}, \quad (3.1)$$

of the *F-h* curve is primarily governing by elastic properties of the material itself (Oliver & Pharr, 1992). It represents the inverse of the system compliance.

The initial unloading stiffness provides the compliance of the indenter and material (the indentation), and the machine. This can be approximated as springs in series, such that the system compliance is given by

$$S = S_{\text{indentation}} + S_{\text{machi}} . \quad (3.2)$$

As the compliance of the material and indenter cannot be modified, the machine compliance needs to be set such that the initial unloading curve of the numerical simulations matches that of experimental data.

A layer of elements was added to the FEM model to serve as the machine compliance. This layer of elements was given an artificial stiffness such that the initial FEM unloading stiffness corresponded to the experimental data. This can be seen in Figure 10, where a stiffness that is too high would produce an overly stiff initial unloading stiffness, and vice versa for a low stiffness with the same  $\sigma$ - $\epsilon_p$  curve. Therefore, the correct element stiffness would need to be determined to match the experimental data.

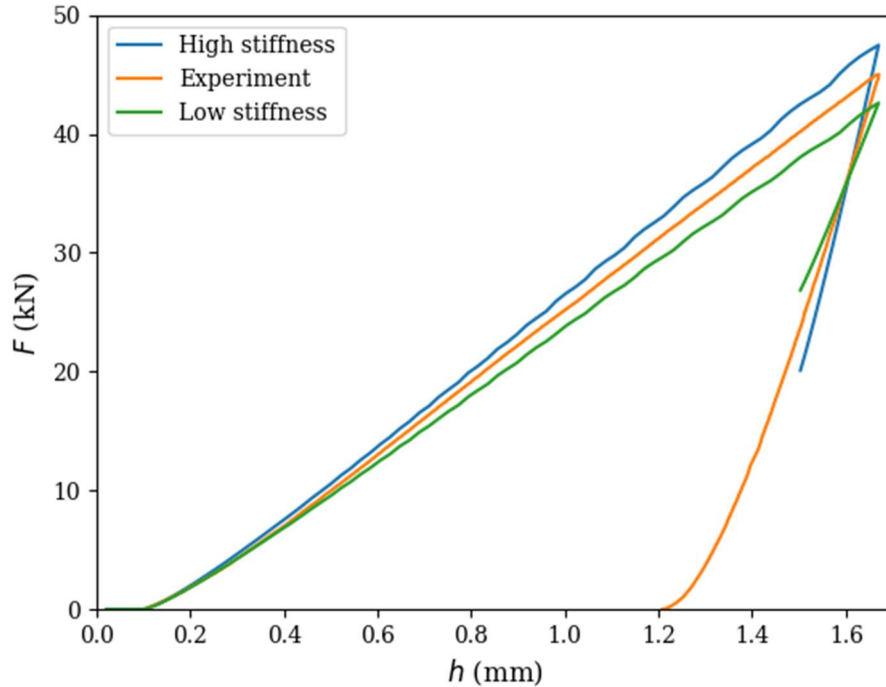


Figure 10 Effect of press stiffness on  $F$ - $h$  curve

#### D. CalculiX Input File

The *CalculiX* input file defines the parameters of the FEM model, and the input cards for *CalculiX* that pertain the indentation test are described in this section.

##### 1. Contact

Contact is implemented in *CalculiX* using the `CONTACT PAIR` input card. Contact is not a topic which was covered extensively in the literature, and the scope of this project does not include the theory of contact. A “rule of thumb” approach was taken, with values being adjusted to where they provided consistent convergence simulation without significantly affecting the output.

The two contact interactions models available in *CalculiX* are linear and exponential. A linear model was used, as only a single parameter would need to be configured, namely the contact stiffness. This contact stiffness is recommended in the *CalculiX* user manual as being 10 times the largest elastic modulus of the two materials undergoing contact (Dhondt, 2016).

The recommended contact stiffness was found to be sufficiently stiff, while still allowing fairly quick convergence of iterations. Using a larger contact stiffness would result in a harder contact which might better represent reality, but it would have the negative effect of slower convergence.

In the implementation of the contact pair, the block was chosen as the master surface, with the indenter being chosen as the slave surface. With the contact pair inverted, the FEM model would not converge. The cause of this is unknown.

Face-to-face contact was used as node-to-face contact would either induce additional numeric noise in the results or the simulation not converge to a solution.

## 2. Friction

Friction is implemented in *CalculiX* using the `FRICITION` input card. A dry friction model is implemented in *CalculiX*. In this model the tangential displacement between the surfaces is characterised by a stick slope for small relative displacements, and then constant slip behaviour thereafter. This behaviour is illustrated in Figure 11. The stick slope,  $\lambda$ , was selected to be 10 times smaller than the contact stiffness, as per recommendation in the user manual (Dhondt, 2016).

Due to the nature of the friction model, simulations which included friction would experience numeric noise due to different regions in under the indenter experiencing stick or slip behaviour at different times. With larger values for the coefficient of friction, the amount of noise would increase. This effect is visible in Figure 12.

Lastly, as highlighted in the literature survey, for larger values for the coefficient of friction the differences in the behaviour of the  $F-h$  curve does in fact become negligible, particularly larger than  $\mu = 0.3$  as seen in Figure 12. Therefore, a value of  $\mu = 0.4$  was chosen for use in all simulations with friction as this roughly corresponds to coefficient values obtained from various sources for friction between steel and aluminium.

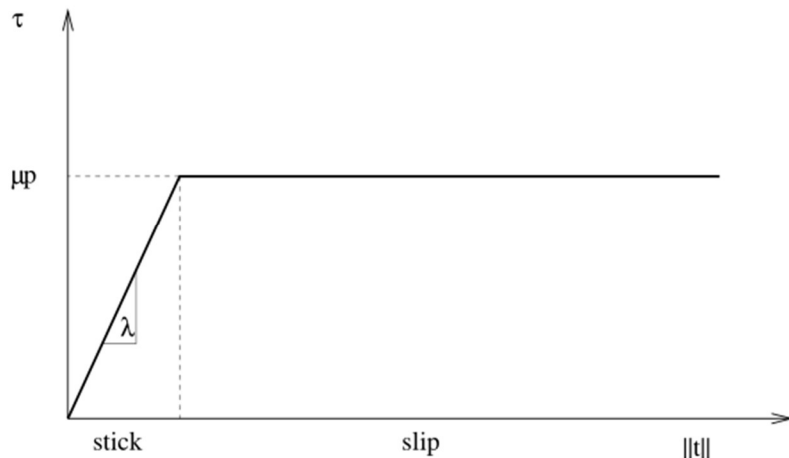


**Figure 11** Shear stress versus relative tangential displacement in *CalculiX* (Dhondt, 2016)

### 3. Plasticity

Plasticity is implemented in *CalculiX* using the PLASTIC input card. The PLASTIC card contains only a single parameter, the hardening rule. *CalculiX* contains built in isotropic and kinematic hardening rules. There is also the option to input a user defined hardening curve.

The default hardening rule in *CalculiX* is isotropic hardening. As the indentation test contains no cyclic loading, this hardening rule should be adequate for modelling plasticity.

The PLASTIC card uses the Von Mises stress to evaluate the yield surface of the material. There are no parameters to modify this behaviour. As failure is not expected to occur, this equivalent stress and strain model should be sufficient.

Lastly, the plasticity card is the entry point for the analysis into the simulations. A stress-strain curve will be drawn up using different methods, which will then be included in the *CalculiX* input file under the PLASTIC card.

### 4. Dynamic Boundary Conditions

While the experiment used force-controlled equipment, the FEM model would be displacement-controlled. This is accomplished by applying a moving boundary condition to the top of the indenter, 12 in Figure 6.

This boundary is moved down to a distance based on the experiment, and then is raised during unloading. In the case with friction present, the FEM model would not be able to break contact, producing negative forces as seen in Figure 12.

These last steps would often triple the simulation time for one simulation. Secondly, without friction it was not possible to match the final unloading shape of the  $F$ - $h$  curve, which can be seen in Figure 19. As such these last few steps were deemed unnecessary.

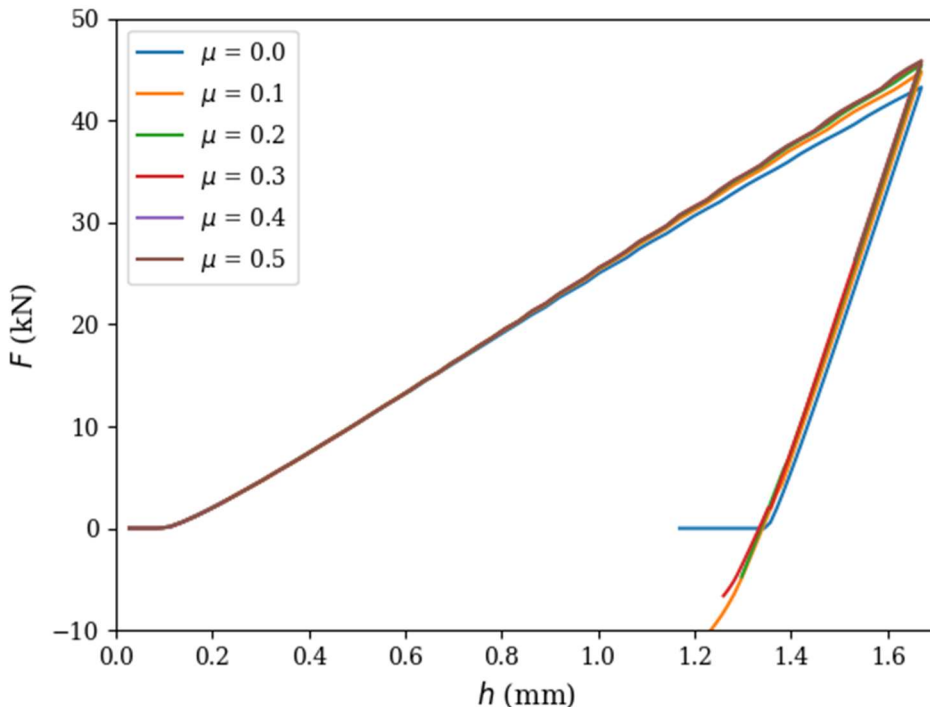


Figure 12 Effects of friction on the  $F$ - $h$  curve

## **E. Numerical Techniques**

When using numerical techniques, existing software packages were used in lieu of implementing an algorithm. This section provides an overview of the techniques and packages used for analysis.

### **1. Direct Minimisation**

For direct minimisation the Nelder-Mead algorithm was used (Nelder & Mead, 1965). The scientific tools for Python library *SciPy* had an implementation of Nelder-Mead algorithm which was used (Jones, et al., 2001).

The Nelder-Mead algorithm, also known as the downhill simplex method, is a derivative-free numerical technique which will iteratively search for a minimum of a function. As the technique is derivative-free, the objective function need not necessarily be smooth. The objective function will contain contact in the FEM model, a highly discrete process, and so its smoothness cannot be determined. While the algorithm may converge slower than derivative based algorithms, such as quasi-Newton algorithms, it offers the advantage of being a potentially more robust method that will more readily converge.

### **2. Database Methods**

Direct minimisation has the caveat that if a different  $F$ - $h$  curve needs to be solved, a new optimisation procedure will need to be done. This is a time-consuming approach. As such, it would be preferable to use a series of known solutions to predict or interpolate new data. These methods are referred to in this report as database methods as they will use information from a database of prior simulations.

#### **a) Radial Basis Function Surrogate Model**

The first form of database methods are surrogate models. Surrogate models seek to approximate the computationally expensive objective function with an inexpensive function in its place, in this case an interpolation function. The choice of surrogate model was a zero order radial basis function surrogate model. The surrogate derives its name from the fact that when using a Taylor series approximation to form the model, only the zeroth order information, i.e. the function values, is used. The zero order model was used to prevent calculating numerical derivatives, which would increase the building time and size of the database.

Surrogate models seek to approximate a function by considering the summation of a number of radial basis functions (RBFs),  $\phi$ , given by Snyman & Wilke (2017) as

$$f(\mathbf{x}) \approx \sum_{j=1}^P w_j \phi_j(\mathbf{x}, \mathbf{x}_c^j) = \bar{f}(\mathbf{x}). \quad (3.3)$$

Here  $f$  is the objective function, typically the mean squared error of the target  $F$ - $h$  curve compared to all the  $F$ - $h$  curves in the database, which is a function of the model parameters,  $\mathbf{x}$ . The radial basis functions are described in detail in Appendix F.

The *SciPy* implementation of RBF surrogate models was used (Jones et. al., 2001).

### b) Statistical Regression

Surrogate models seek to approximate an objective function in terms of the parameters,  $\mathbf{x}$ , by considering the sum of many weighted individual functions. An alternative approach would be to find some linear map that would relate the experimental  $F$ - $h$  data,  $\mathbf{x}$ , to the desired  $\sigma$ - $\varepsilon_p$  data vector,  $\mathbf{y}$ , with some linear mapping matrix,  $\mathbf{b}$ , with some error vector,  $\mathbf{e}$ , or

$$\mathbf{y} = \mathbf{x}\mathbf{b} + \mathbf{e}. \quad (3.4)$$

This is commonly known as multiple linear regression analysis. However, equation (3.4) only maps one vector to another. It may be preferable to use an entire database to “train” the regression and form the  $\mathbf{b}$  matrix, and such techniques are known as statistical learning or machine learning. One such technique explored is partial least squares (PLS). PLS will combine all the observed independent variables, depended variables, and errors into matrices, or simply all the individual vectors in equation (3.4) added together into the form

$$Y = XB + E. \quad (3.5)$$

Here, for a dataset of  $n$  observations,  $Y$  is a  $p \times n$  matrix,  $X$  is a  $n \times m$  matrix and  $B$  is a  $m \times p$  matrix. The lengths of the  $\mathbf{y}$  and  $\mathbf{x}$  vectors,  $p$  and  $m$  respectively, are entirely dependent on the problem and chosen variables. The  $B$  matrix then represents a linear map which is then used to predict some  $Y$  data with new  $X$  data.

In its underlying model, PLS seeks to find the mean values of the output training data, then quantify the variance from these mean values with respect to corresponding input training data. A more detailed description on PLS is given by Geladi & Kowalski (1986).

The Python machine learning software package *scikit-learn* is used with its implementation of PLS (Pedregosa, et al., 2011).

## V. EXPERIMENTAL PROBLEM

This section outlines the stress-strain models which would provide the best possible matches to the experimental  $F$ - $h$  curve. When using experimental data however, some limitations were imposed on the analysis.

### A. Exclusion of Surface Profile

When friction was added to the model, the indenter could not be fully extracted from the model. This has the implication that to match the experimental data, the surface profile cannot be used.

If some factor was found that would relate the friction model to the frictionless model, friction could be removed and the surface profile could be used. However, the effect of friction could neither be reduced to a scaling or additive curve. Figure 13 shows the ratio of the  $F$ - $h$  loading curve with friction to its corresponding curve without friction for four random  $\sigma$ - $\varepsilon_p$  curves. No trend is found among even with these few data sets. As such, in order to model the problem with friction, the surface profile could not be successfully used with the experimental data, and only the  $F$ - $h$  data could be used.

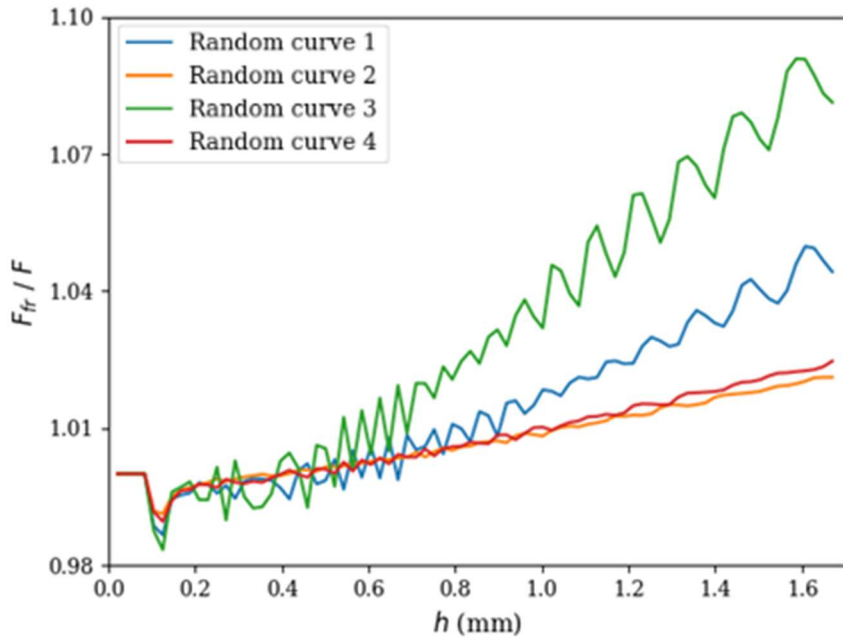


*Figure 13 Ratio of friction and frictionless  $F$ - $h$  loading curves for random  $\sigma$ - $\varepsilon_p$  curves*

### B. One Parameter Model

To serve as an introduction to applying material models, a single parameter model was explored, namely a modified Holloman power law relationship. The stress-strain relationship is in terms of a single unknown exponent  $n$  and is given by Taljat, et al. (1998) as

$$\sigma(\varepsilon_p) = \sigma_0 \left( \frac{\sigma_0}{E} \right)^{-n} \left( \varepsilon_p + \frac{\sigma_0}{E} \right)^n. \quad (4.1)$$

In order to find a solution which will match the stress strain curve, some criterion will need to be met. The proposed criterion is of the form

$$f(h, n) = F, \quad (4.2)$$

where the function  $f$  is the numerical  $F$ - $h$  output of the simulation. In order to solve this equation, numerical methods will need to be employed, which will take the form of a root-finding problem.

As the function  $f$  is unknown and requires a numerical approach, bracketing methods were used, namely the bisection method. However, equation (4.2) is not suitable for the bisection method as it is a three-dimensional root finding problem. In order to constrain the problem, the maximum force from the simulation is compared to the known maximum force from experimental data,  $F_{max}$ . This simplifies the root-finding problem to a two dimensional problem, and given by

$$\max(f(n)) - F_{max} = 0. \quad (4.3)$$

For this model, a yield stress of 250 MPa was assumed. Table 2 lists the parameter values obtained for the found minimum solution. Figure 14 shows the  $F$ - $h$  curves of the experimental and model data.

**Table 2** Optimal one parameter model's parameters

Parameter	Value
$\sigma_0$	250 MPa
$E$	70 GPa
$n$	0.1169

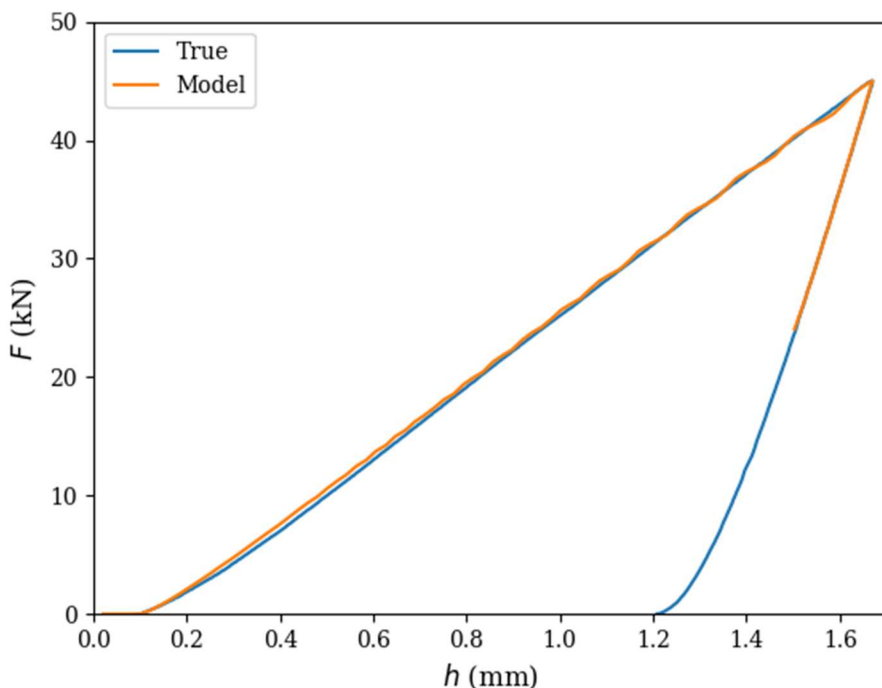


**Figure 14**  $F$ - $h$  curve for one parameter model

### **I. Analysis of One Parameter Model**

The one parameter model successfully served as an introduction for the application of numerical methods to the problem, and was simple to both setup and analyse. It also produced a surprisingly good fit for the data, as one parameter models are typically only suitable for few families of materials. However, there are visible deviations in the shape of the  $F$ - $h$  curve, which suggests that more model parameters may be needed.

The method used with the one parameter model cannot easily be extended to a two, or higher, parameter model, as this creates a three dimensional root finding problem. Bracketing methods cannot be used in three-dimensional root finding methods. One alternative would be to use Broyden's Method, a 3-dimensional generalisation of the secant method. However, using root finding will not be an appropriate method when trying to approximate an entire curve rather than selected points. Furthermore, uniqueness is not guaranteed and likely impossible as only a few data points will be used with increasingly flexible models. Therefore, minimisation of some evaluation criterion for the entire curve was used for higher parameter models.

### **C. Evaluation Criterion for Entire Curve**

As more parameters are added to the stress strain model, a more sophisticated evaluation criterion is needed to analyse a curve rather than a single point. The proposed general criterion for evaluating some set of data is the mean squared error, which is given by

$$e^{(\phi)} = \frac{1}{n} \sum_{i=1}^n (\hat{\varphi}_i - \varphi_i)^2, \quad (4.4)$$

where  $\hat{\varphi}$  is a predictor value for some predetermined data, and  $\varphi$  is the FEM observed value, and  $n$  is the number of observations. The predictor and observed values would typically be the force at a particular displacement in the loading curve at  $n$  points along the loading curve of the FEM and experimental  $F$ - $h$  curves respectively.

In application, the minimisation would be in terms of a vector of the model parameters,  $\mathbf{x}$ , and the objective function  $f$  will be a linear combination of the mean squared errors for the loading curves and the surface profiles, or

$$\min_{\mathbf{x}} f(\mathbf{x}) = \min_{\mathbf{x}} (e^{(Fh)} + w e^{(rh)}). \quad (4.5)$$

The weighting factor,  $w$ , was generally set to 0, such that only the  $F$ - $h$  curve was considered, or set appropriately to ensure that both the  $F$ - $h$  and  $r$ - $h$  errors were at approximately the same order of magnitude.

### **D. Higher Parameter Models**

The one parameter model could match the  $F$ - $h$  curve to an extent, but improvements could be made as it did not match the data exactly. Higher parameter models were explored to see if the indentation test provides sufficient information to describe the  $\sigma$ - $\varepsilon_p$  curve with more detail.

### 1. Two Parameter Model

The two parameter material model used was a reduced three parameter model. Naturally, this will require some a priori knowledge of the plasticity of the material as with the one parameter model. In this model, the yield stress,  $\sigma_0$ , of the material is again assumed, as it is typically one of the plastic properties of a material given by manufacturers. Kucharski & Mroz (2007) also present an analytical procedure which can be used to determine the yield stress from a spherical indentation test. A yield stress of 250 MPa was assumed.

The proposed two parameter model used, also known as Ludwik's equation, is a power law relationship adapted for use with plastic strains. The model is given as

$$\sigma(\varepsilon_p) = \sigma_0 + K\varepsilon_p^n. \quad (4.6)$$

Table 3 lists the parameter values obtained for the found minimum solution. Figure 15 shows the  $F$ - $h$  curves of the experimental and model data.

*Table 3 Optimal two parameter model's parameters*

Parameter	Value
$\sigma_0$	250 MPa
$K$	585.5
$n$	0.7487

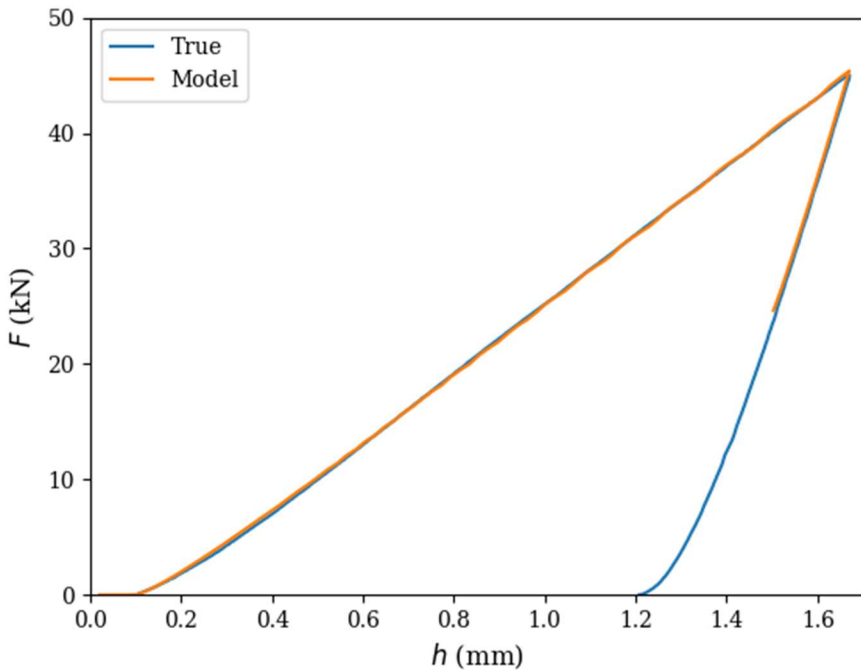


*Figure 15 F-h curve for two parameter model*

The two parameter model does indeed offer a better fit compared to the one parameter model. However, there are still discrepancies in the data, and as such a three parameter model was investigated to see how much additional benefit there is with higher parameter models.

## 2. Three Parameter Model

Thus far, only power law based models have been explored. While power law models are widespread, they may not be applicable for many materials. Power law relationships are typically applicable to body-centred cubic metals, while face-centred cubic metals, such as aluminium, are more well modelled using saturation based laws (Sung, et al., 2010). One such relationship was proposed by Voce (1948). The relationship is given by the differential equation

$$\frac{d\sigma}{d\varepsilon_p} = \theta_0 \left( 1 - \frac{\sigma}{\sigma_s} \right). \quad (4.7)$$

Here,  $\theta_0$  represents the initial work hardening rate, and  $\sigma_s$  represents the saturation stress of the material. The close form solution for equation (4.7) is

$$\sigma(\varepsilon_p) = \frac{\sigma_0}{1 - b} (1 - be^{-m\varepsilon_p}). \quad (4.8)$$

In this model,  $m$  is the initial work hardening rate constant. The saturation stress is defined by the saturation constant  $b$ , or

$$\sigma_s = \frac{\sigma_0}{1 - b}. \quad (4.9)$$

Table 4 lists the parameter values obtained for the found minimum solution. Figure 16 shows the  $F$ - $h$  curves of the experimental and model data.

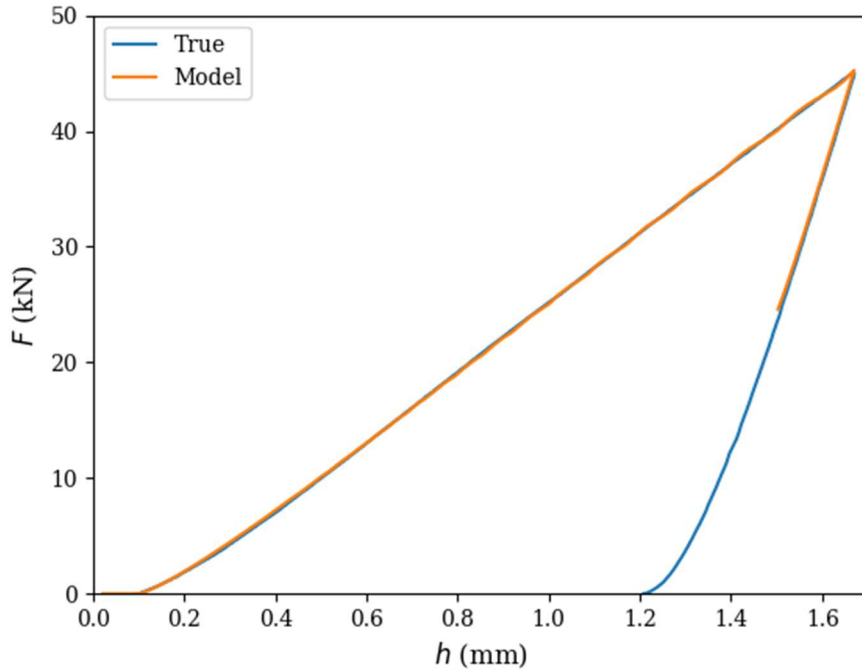


Figure 16  $F$ - $h$  curve for three parameter model

Figure 16 shows that there is an improvement compared to the two parameter model in Figure 15. The improvement in matching the  $F$ - $h$  curve less noticeable though, which shows that a point of diminishing returns is being reached.

There are still minor discrepancies at lower indentation depths. It is possible that these are due to effects in the hydraulic press which are unaccounted for.

*Table 4 Optimal three parameter model's parameters*

Parameter	Value
$\sigma_0$	204.6 MPa
$b$	0.6214
$m$	9.107

Lastly, when using the three parameter model, a yield stress of 204 MPa was obtained. This is significantly lower than the manufacturer provided yield stress of 250 MPa as used in the previous models. This is the first model where the yield stress was not fixed, but one would expect it to rise as manufacturer given yield stresses are typically guaranteed minimum yield stresses. Uniaxial tests showed a minimum yield stress value of around 280 MPa.

### 3. Four Parameter Models

Two four parameter models are presented. Both models are based on the three parameter Voce relationship. First is the inclusion of a non-saturating term in the model, given by

$$\sigma(\varepsilon_p) = \frac{\sigma_0}{1-b}(1 - be^{-m\varepsilon_p}) + E_p \varepsilon_p. \quad (4.10)$$

A linear term is present in this model which causes the model to saturate towards a tangent modulus,  $E_p$ , rather than a saturation stress. The model may better model behaviour at large plastic strains for real materials.

In the FEM model large maximum plastic strains are obtained, but the bulk of the plastic strain is still at relatively low values. As such, it may be beneficial to use a material model which will increase the flexibility of the  $\sigma$ - $\varepsilon_p$  curve at lower strains. The proposed model consists of a constant stress component and an evolving stress component, given by

$$\sigma = \sigma_0 + \sigma_e. \quad (4.11)$$

The evolving strain component is a modification of the differential form of the Voce model, given by introducing an exponent,  $n$ :

$$\frac{d\sigma_e}{d\varepsilon_p} = \theta_0 \left(1 - \frac{\sigma_e}{\sigma_s}\right)^n. \quad (4.12)$$

This four parameter model should be more suitable for the problem. There is no simple closed form analytical solution for this non-linear differential equation, and so a numerical differential equation solver was used to obtain the  $\sigma$ - $\varepsilon_p$  curve using this model.

When optimising for either model directly at a variety of starting points, two major difficulties were present. The algorithm would often fall into a local minimum, producing an error greater than that of the three parameter model. When the model managed to optimise to an improved solution, the solutions were only marginally better than the three parameter model, i.e. typically only a 5% decrease in the  $F$ - $h$  curve mean squared error compared to the three parameter model, with the  $F$ - $h$  curves being visually indistinguishable.

The unreliability of directly using four parameter models suggests one of two major problems:

- The four parameter model produces changes that are so fine that the optimisation algorithm primarily matches the data to numerical or experimental noise rather than overall shape.
- The indentation test as is does not provide a sufficient amount of information about the  $\sigma$ - $\varepsilon_p$  curve for four and higher parameter models to be used.

### E. Comparison of Models

One can see by comparing Figures 14, 15, and 16 that an increase in number of model parameters does improve the fit of the  $F$ - $h$  curve. Table 5 gives relative mean squared errors of the  $F$ - $h$  curves compared to the one parameter model are shown in Figure 14.

*Table 5 Relative minimum error of different models*

Number of Parameters	Relative Error
1	1
2	0.201
3	0.100

The aim of material identification is to identify the material, not to match the  $F$ - $h$  curve alone. The  $F$ - $h$  error does in fact decrease as the model complexity is increased, and so one would expect the corresponding  $\sigma$ - $\varepsilon_p$  curves to converge towards the true solution. However, Figure 17 shows that the  $\sigma$ - $\varepsilon_p$  curves for the models do not converge towards a single curve.

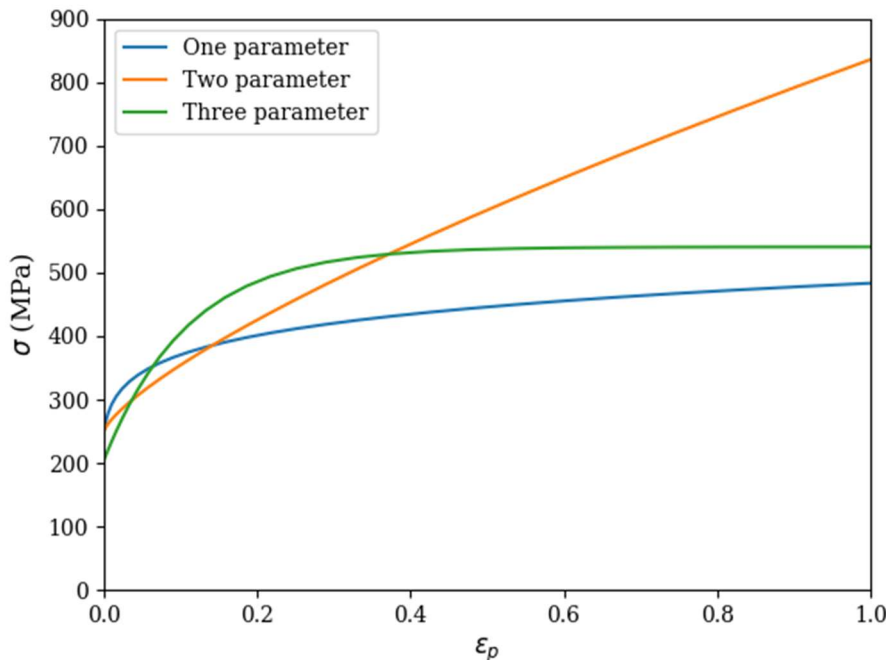


*Figure 17*  $\sigma$ - $\varepsilon_p$  curves for different models

Figure 18 shows the two most varying experimental  $F$ - $h$  curves alongside the one and three parameter models. Figure 19 shows a section of the  $F$ - $h$  curves. It was observed that the three parameter model was always within the band of the experimental data. The one parameter model went outside this band of values, but not by a significant amount.

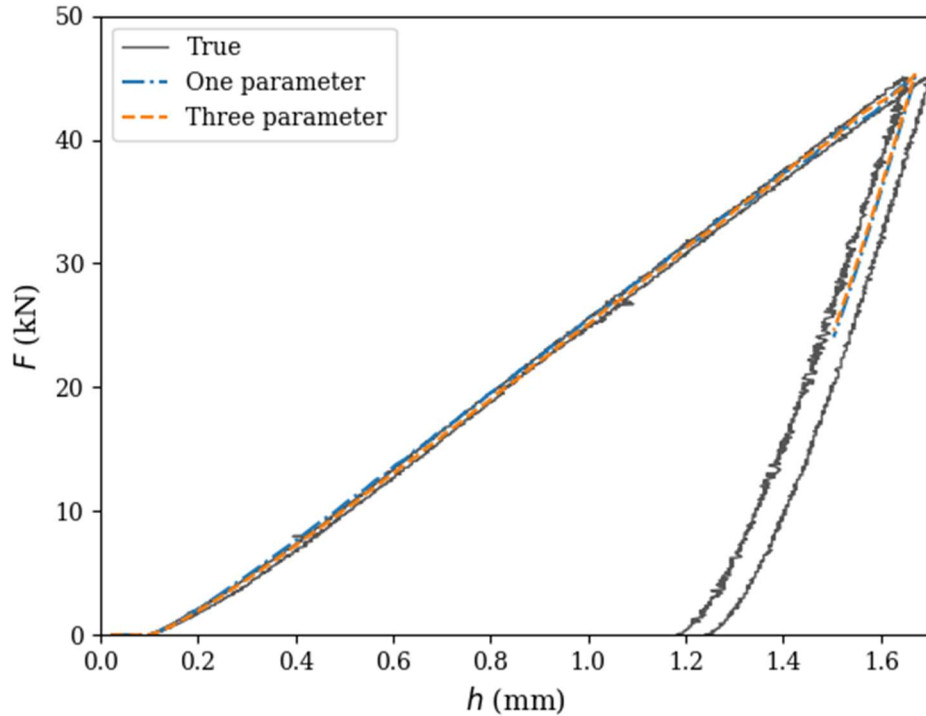


**Figure 18** Models compared to bands of experimental data

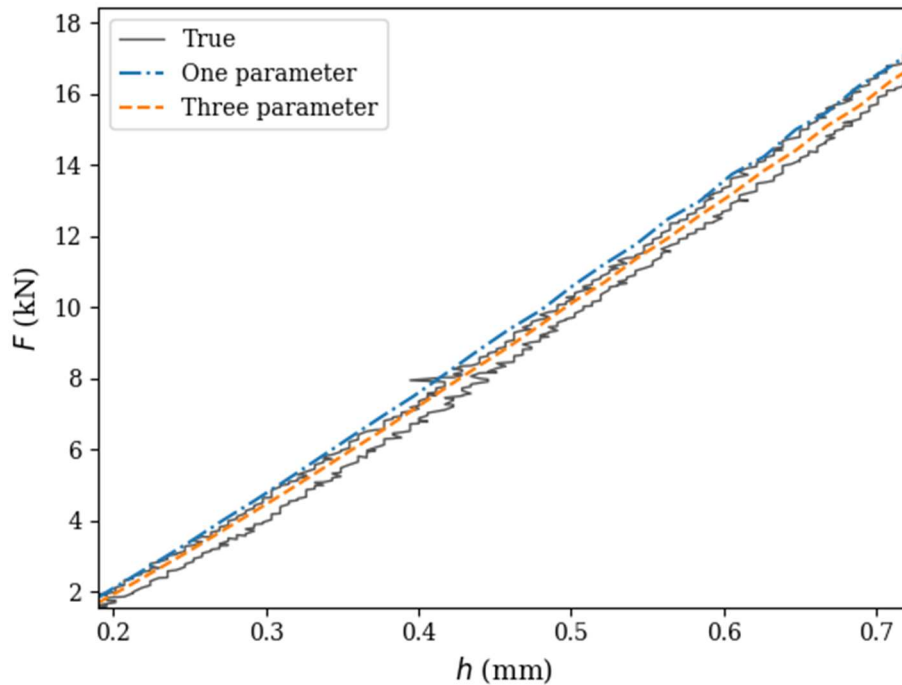


**Figure 19** Detail view of models compared to bands of experimental data

Despite the fact that the FEM model was consistent, all three models produced  $F$ - $h$  curves were comparable to the spread of experimental data while producing different and non-converging  $\sigma$ - $\epsilon_p$  curves. This creates concerns about uniqueness of the problem.

Lastly, looking again at Figure 4, the experimental  $F$ - $h$  curves are of a similar shape, with the majority of deviation at the larger displacements. The models could accurately match the later portion of the loading curves, while struggling to match the portion of the curve where experimental data was more consistent. This suggests that the FEM model could have experimental influences which are unaccounted for.

#### ***F. Comparison with Frictionless Model***

A frictionless model was run using the same  $\sigma$ - $\epsilon_p$  curve obtained for the three parameter model with friction. Figure 20 shows the  $F$ - $h$  curves for both of these simulations alongside the experimental data. It can be noted that the inclusion of friction only influences the second half of the loading curve.

Figure 20 also shows that when the indenter is nearly unloaded, there is a large difference in the shape of the unloading curves between the FEM model and the experimental data. The cause of these discrepancies is unknown, and could be attributed to surface interaction effects or influences from the experimental equipment.

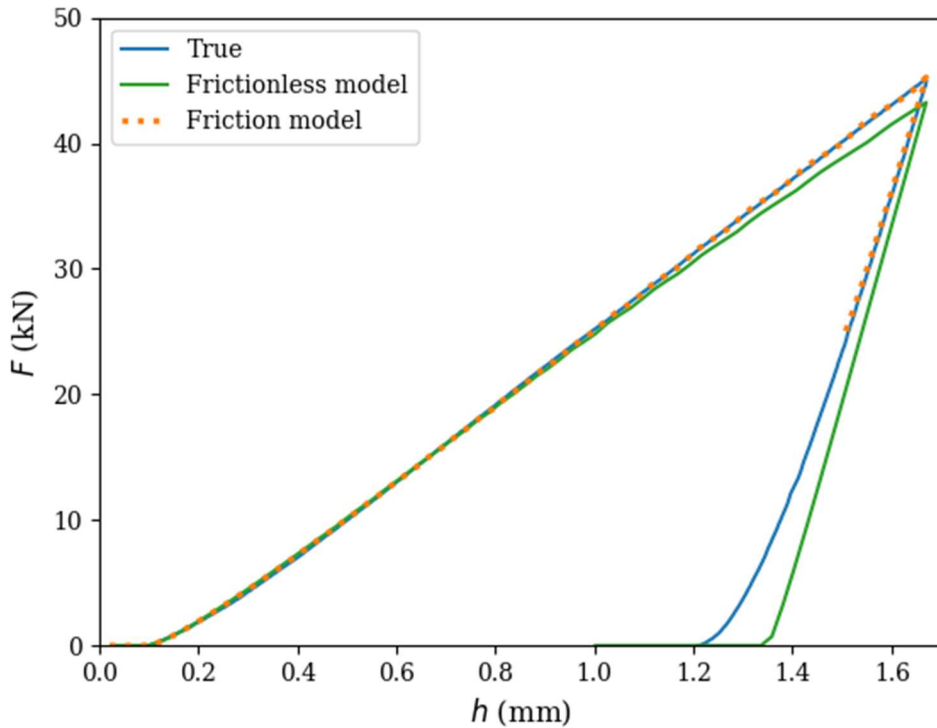


**Figure 20**  $F$ - $h$  curves for friction and frictionless three parameter model

The surface profile could be extracted from the frictionless model and compared to the experimental surface profile. As the FEM model did not have the same final indentation depth as the experiment data, the surface profile had to be normalised with respect to the real surface profile in some way.

To normalise the surface profile, it was either shifted up or a scaling factor was applied to ensure that the final depths were equal. Figure 21 shows the three surface profiles.

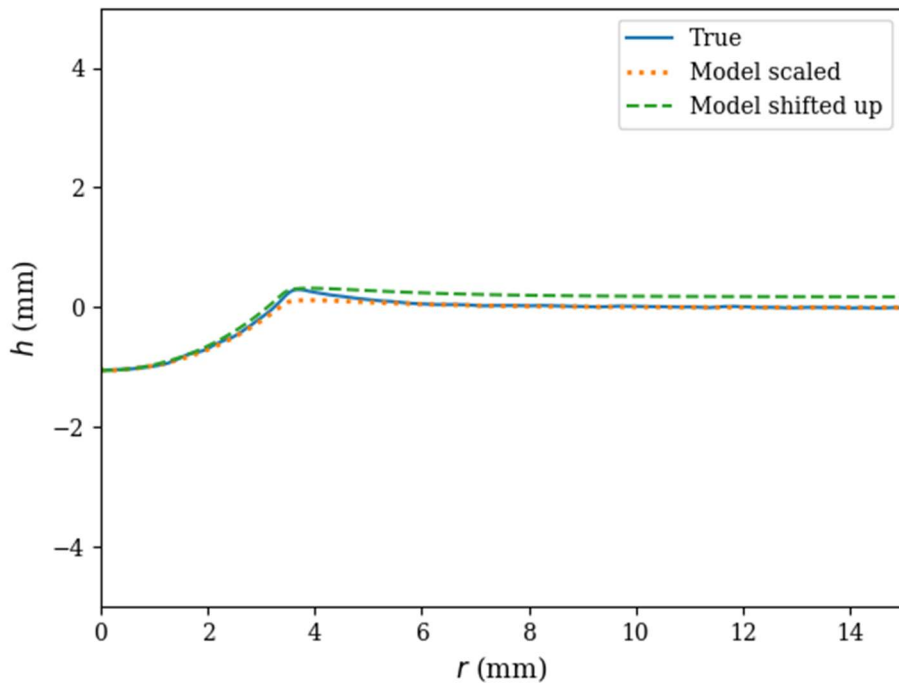


**Figure 21** Surface profile for frictionless three parameter model

It can be seen that the frictionless surface profile is not similar to the experimental surface profile with regardless of normalisation method. However, both the experimental and numerical surface profiles have the same ridge-peak diameter as the experimental data.

The lack of similarity is likely attributed to a lack of friction in the model. If this discrepancy is not caused by friction, it will raise more questions about the uniqueness of the problem, as the  $F$ - $h$  curve can be sufficiently matched but not the surface profile.

#### G. Effect of Indenter on $F$ - $h$ Curve

The indenter was modelled with a boundary condition placed in an area with notable stress and strain variations, and so it may influence the behaviour of the indenter.

For the three parameter model, the optimal yield stress was below that of the manufacturer provided yield stress. This discrepancy could be due to the fact that the indenter could behave excessively rigidly, and so the sample material will need to soften during deforming to match the experimental data. To test this, the full indenter and the indenter holder were modelled, as seen in Figure 22.

The compliance of the machine compliance layer in the model was adjusted to allow for the increased compliance in the system due to the larger indenter volume. The  $F$ - $h$  curves for the original and modified indenters are shown in Figure 23. Also included is the  $F$ - $h$  curve when a rigid indenter is used, again adjusting for the machine compliance for the now decreased compliance in the indenter.

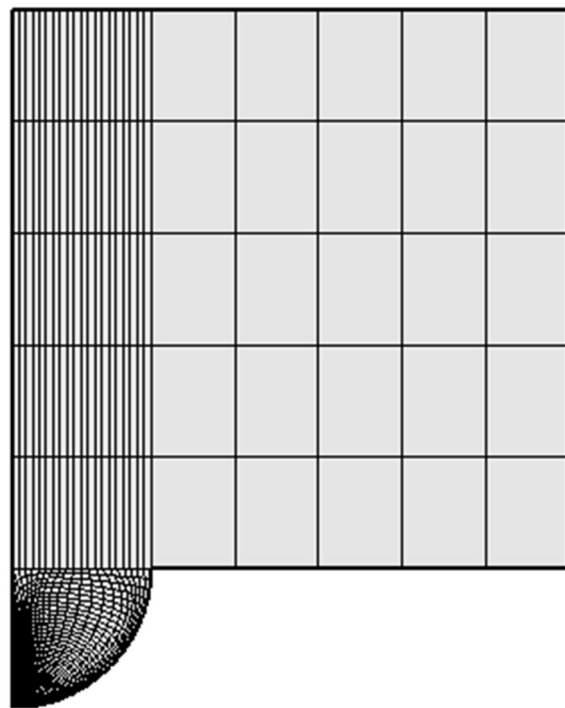


**Figure 22** FEM model of indenter and holder

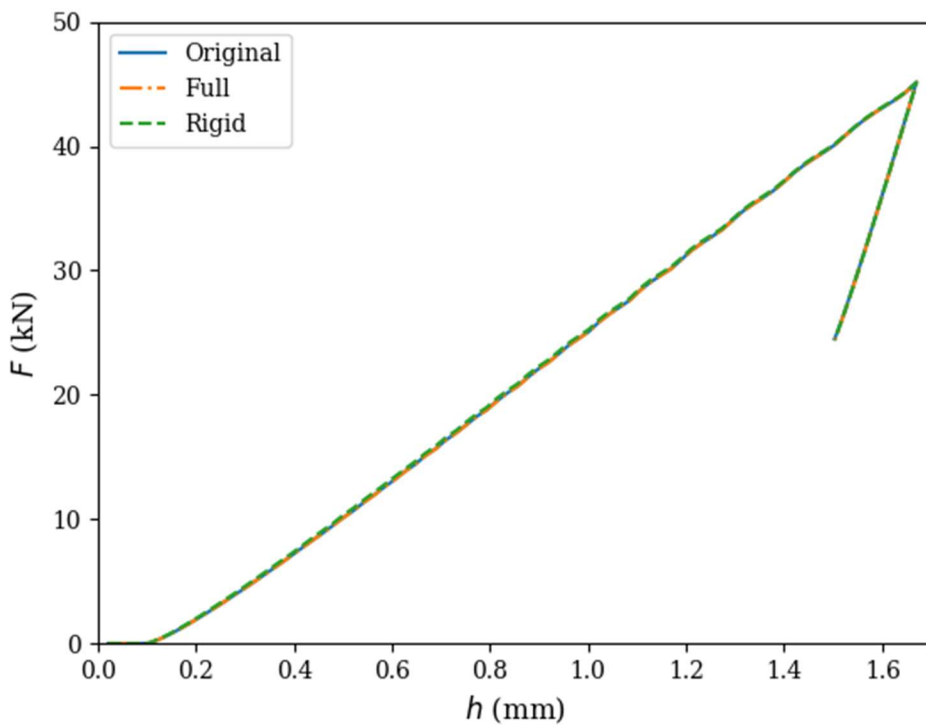


**Figure 23**  $F$ - $h$  curves for different indenter models

It can be seen in Figure 23 that no notable deviation occurred when using the full indenter and holder compared to the original hemispherical indenter. The two curves are essentially superimposed.

When modelling the indenter as a rigid body, small deviations occurred between 0.4 and 1.0 mm in the indentation. The magnitude of these deviations are small, but they do influence the shape of the  $F$ - $h$  curve, i.e. the final 0.2 mm loading of the indentation are still identical to the original indenter. These affects are well within the margin of error for experimental data though.

As such, modelling the indenter as a non-rigid hemisphere appears to be sufficient for this problem.

#### **H. Uniqueness of Problem**

It was found during optimisation of the three parameter model that the algorithm would often converge rapidly towards a point, and then then slowly start to move towards a different point without significant changes in the  $F$ - $h$  curve's mean squared error between iterations. During this, only two of the parameters would vary. This is indicative of a poorly posed optimisation problem, as it shows the presence of a valley. A grid of simulations was done for a fixed saturation stress constant, and can be seen in Figure 24. The contours are the mean squared error of the  $F$ - $h$  curve relative to the error of the final three parameter model as shown in Figure 16.

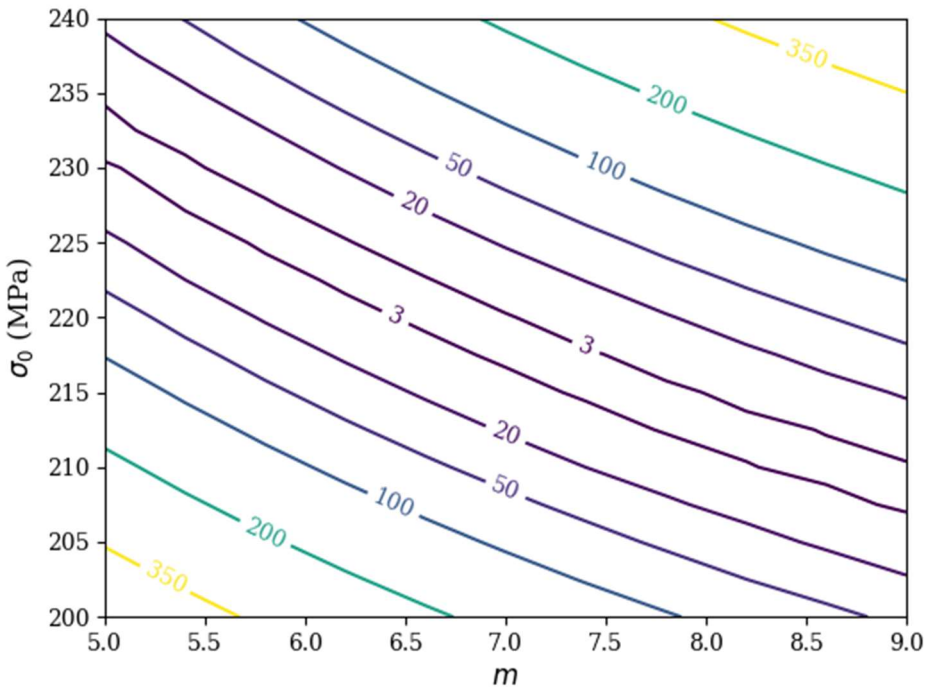


**Figure 24** Contour plot of the relative  $F$ - $h$  MSE with fixed saturation constant

As per Table 5, any relative error less than 10 is still an improvement over the one parameter model, and will likely be within the bands of the experimental error as per Figure 18. A valley can clearly be seen in the solution for error values below this, showing a line of solutions within experimental error. This certainly brings the uniqueness of the problem with the experimental data into question.

## I. Pitfalls of Experimental Data

If the yield stress of the material is allowed to be varied, it optimises towards stresses which are significantly lower than the manufacturer supplied yield stresses and uniaxial test data estimates.

A cause for the discrepancy in the yield stress may be due to plastic affects in the indenter itself. Figure 25 shows the stress distribution in the indenter for the three parameter model solution at the maximum indentation depth.

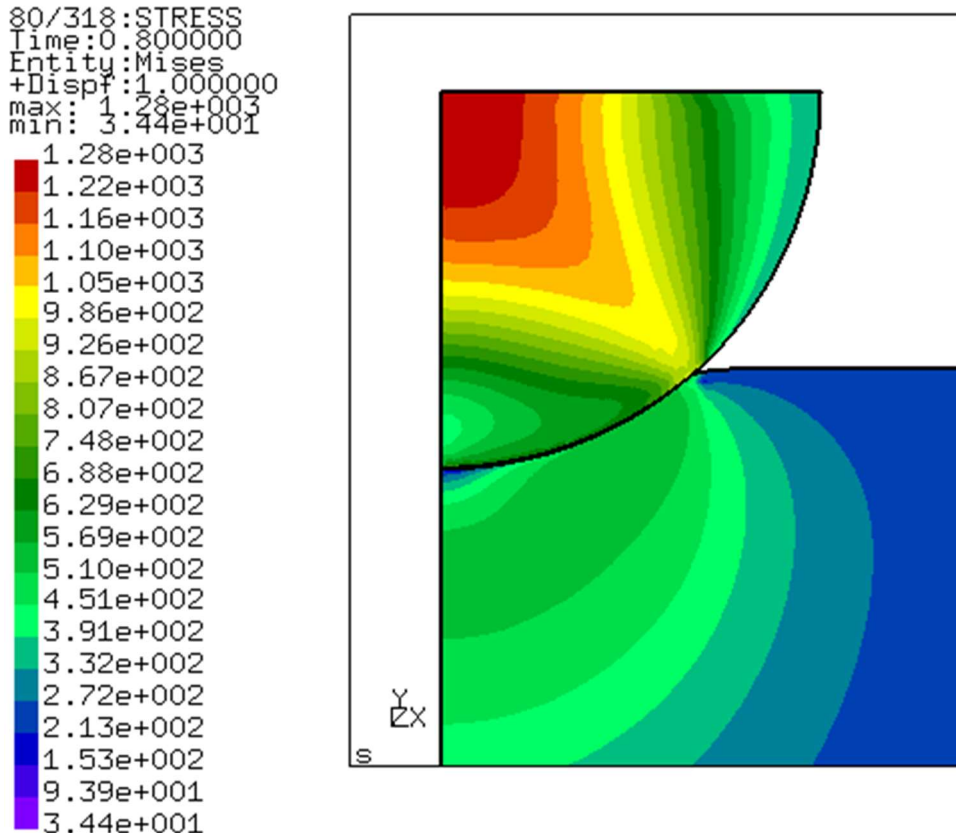


*Figure 25 Stress distribution in indenter*

It can be seen that the largest stress occurs in the indenter rather than the material. A maximum stress of 1280 MPa is observed in the indenter. This stress occurs near the boundary conditions, and so the experimental indenter may have experienced different stresses.

These stresses are still significant, and as the grade of steel used in the ball bearing indenter was not known it is possible that plastic deformation may have occurred in the centre of the indenter. If the problem were to be solved using the obtained experimental data with a plastic-deforming indenter, two  $\sigma$ - $\varepsilon_p$  curves would need to be found. This would likely be impossible to solve for uniquely.

Lastly, the FEM model of the problem may be lacking some of the appropriate physics of the real problem. Examples of this are the poor friction model implemented in *CalculiX* and the fact that there is a section of the  $F$ - $h$  curve that none of the models could match between 0.2 and 0.4 mm.

## VI. VIRTUAL PROBLEM

Numerous difficulties were found trying to match the experimental data. Instead of trying to solve the problem with real data, one could solve a virtual problem where the exact solution is known beforehand.

While the virtual problem may only have a limited physical resemblance to a real problem, it offers the ability to mitigate many ill-modelled aspects of the problem, such as friction, experimental noise, or potential plasticity in the indenter.

### A. Direct Optimisation with Surface Profile

As friction was excluded for the virtual problem, this meant that the indenter could be fully extracted from the surface of the sample, and so the surface profile could be consistently used. This creates the question of what is the effect of including the surface profile in the objective function for direct minimisation.

To test this, an arbitrary power law curve based on equation (4.6) was selected as the true solution, and a three parameter saturation model as described in section V.D.2. was selected to try and match it. The mean squared errors for the  $F$ - $h$  curve, the surface profile, and the  $\sigma$ - $\varepsilon_p$  curves were recorded. These curves were all set such that the initial errors were 1 and all successive errors were made relative to the initial error. Figure 26 shows the relative  $F$ - $h$  errors at each of the objective function evaluations during the optimisation. Figures 27 and 28 show the relative mean squared errors for the surface profile and  $\sigma$ - $\varepsilon_p$  curves respectively.

It should be noted that regardless of the inclusion of the surface profile, after around 100 iterations the true and estimated  $F$ - $h$  curves and surface profiles would be visually identical. However, for the purposes of comparing the effect of including the surface profile, only the numerical values themselves are compared.

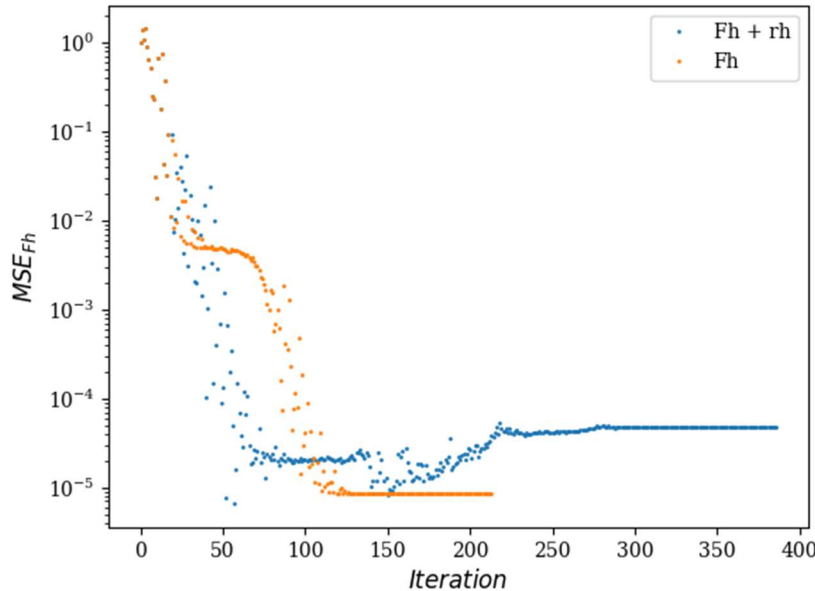


**Figure 26** Relative MSE for  $F$ - $h$  curve

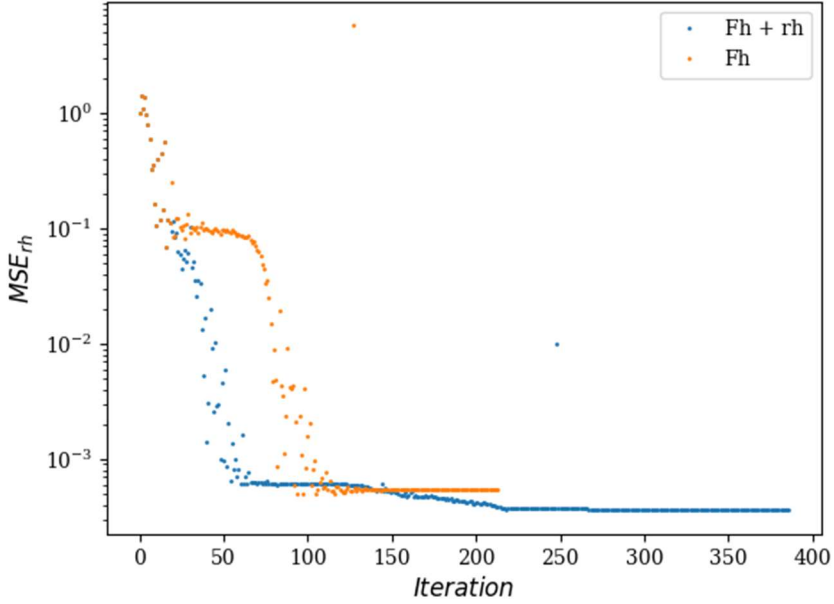


**Figure 27** Relative MSE for surface profile

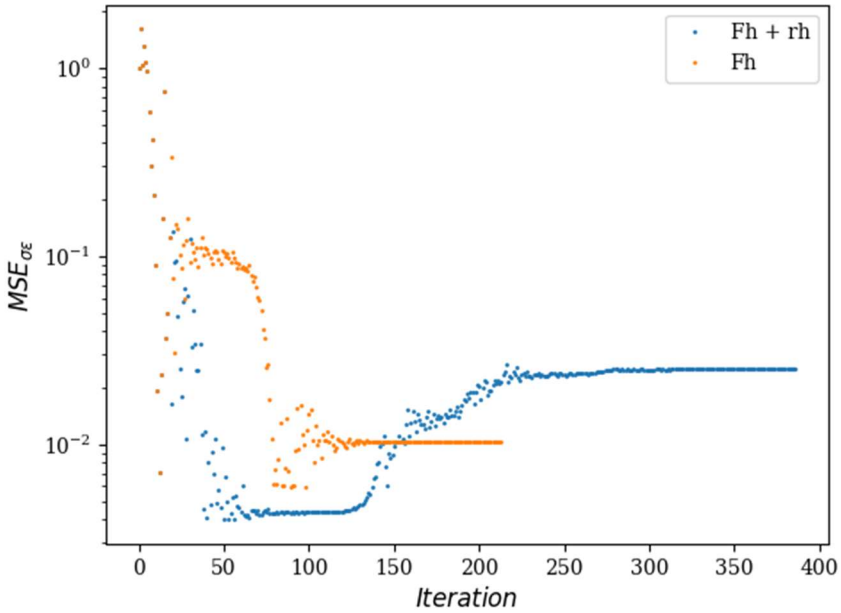


**Figure 28** Relative MSE for  $\sigma\text{-}\epsilon_p$  curve

Figure 26 shows the inclusion of the surface profile results in a larger final error for the  $F\text{-}h$  curve. This is to be expected as the objective function now has to find a compromise between the  $F\text{-}h$  curve and surface profile. Figure 27 confirms this, as a smaller error is obtained for the surface profile.

However, in terms of matching the  $\sigma\text{-}\epsilon_p$  curve, the inclusion of the surface profile slowly moves away from a better estimate to a worse as seen in Figure 28. This indicates that including the surface profile in the direct optimisation has the possibility of producing a worse  $\sigma\text{-}\epsilon_p$  curve estimate, while taking nearly twice as long to converge to a solution.

It appears that the inclusion of the surface profile dramatically increases the initial minimisation rate. If this is true in general, the inclusion of the surface profile may be used to more quickly find a working solution after which only the  $F$ - $h$  curve may be considered. To test this, several random starting points were chosen and ran for 50 objective function evaluations. The results are given in Appendix G. It was found that there is no apparent trend in terms of the rate of minimisation.

The greater error solution and no trends in performances improvement suggests that unless the weighting between the  $F$ - $h$  curve and surface profile is modified or added in the objective function in some other way, the inclusion of the surface profile may be detrimental to direct optimisation.

### B. Parameterisation of Problem

When analyzing the effect of including the surface profile, the three parameter model was used to fit to a power law curve described by equation (4.6). This was done as the two material models would not be able to exactly match each other, as they are not of the same mathematical form. The results of the direct optimisation in the previous section are given here. Figure 29 shows the true objective power law  $\sigma$ - $\varepsilon_p$  curve with the least squares fit and the directly optimised three parameter model  $\sigma$ - $\varepsilon_p$  curves, and Figure 30 shows the true and directly optimised  $F$ - $h$  curves.

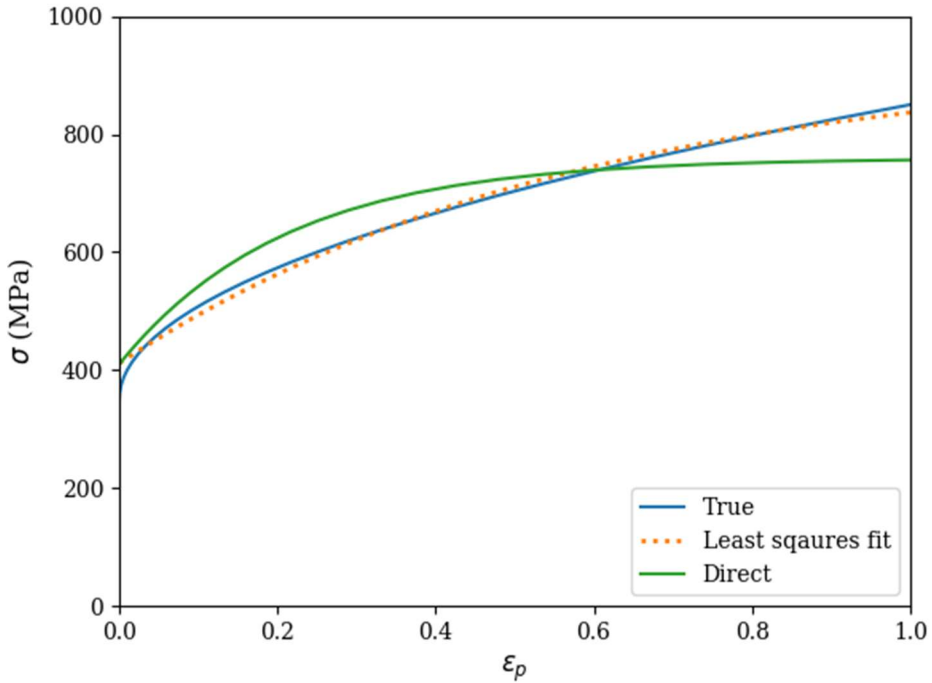


Figure 29  $\sigma$ - $\varepsilon_p$  curves for mapping three parameter model to power law curve

A real material will most likely have a  $\sigma$ - $\varepsilon_p$  curve which cannot be fully described by the three parameter model. The fact that the  $F$ - $h$  curve, as shown in Figure 30, is met with a models of different forms shows that three parameters are all that may be needed to meet a virtual  $F$ - $h$  curve.

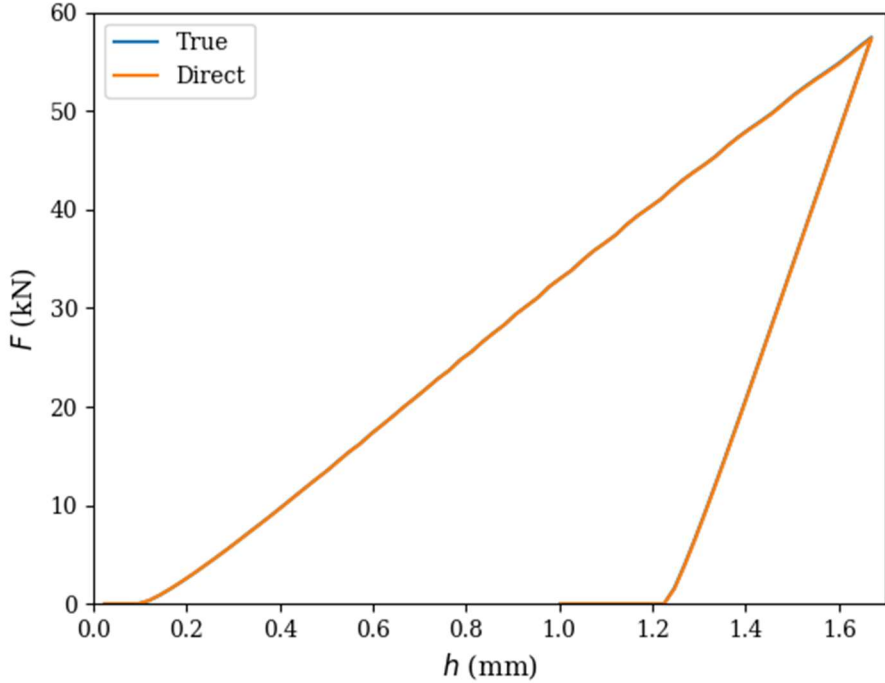


Figure 30  $F$ - $h$  curves for fitting three parameter model to power law curve

Figure 30 shows that the  $F$ - $h$  curves are essentially superimposed on one another. However, when considering Figure 29, the  $\sigma$ - $\varepsilon_p$  curve determined with direct optimisation is not the true best fit. The  $\sigma$ - $\varepsilon_p$  curves are significantly different between plastic strains of 0.1 and 0.5, where the majority of plastic strains are found. This means that it is possible to optimise for a curve in which the result is not the best approximation of that curve. This brings the picture of uniqueness into question for the virtual problem, and through extension to the overall problem of using the  $F$ - $h$  data from an indentation test to determine the  $\sigma$ - $\varepsilon_p$  curve of a material.

### C. Database Sampling

The database techniques will now be explored, and so the construction and sampling of the databases should be considered. There are many factors which will influence the performance of the database, such as the centre, the range, and the distribution of the database.

There is also the matter of the form of the data which will populate the database. The surrogate model is constructed in terms of the  $\sigma$ - $\varepsilon_p$  model parameters, and so it requires that every entry in the database be expressed in terms of these parameters, i.e. have the same  $\sigma$ - $\varepsilon_p$  model. While statistical regression techniques can be used with the parameters, it may be more beneficial to rather map the  $F$ - $h$  curve to the  $\sigma$ - $\varepsilon_p$  curve directly. This would allow a database to be formed using a variety of different models, which will have the effect of training the algorithm with a wider variety of data, potentially making the algorithm more robust for completely unknown  $\sigma$ - $\varepsilon_p$  curves.

Two databases were constructed using the three parameter model centred about the parameters shown in Table 6. The range of the databases is set to  $\pm 25\%$  of the centre parameters.

**Table 6** Centre for databases

Parameter	Value	Range
$\sigma_0$	350	262.5 – 437.5
$b$	0.5	0.375 – 0.625
$m$	5	3.75 – 6.25

Two distributions were used for the databases. One was a uniformly spaced database, with the combinations of six values being taken for each parameter, producing a database of 216 entries. The other database consisted of 256 entries generated using Latin hypercube sampling (LHS). LHS is a random sampling technique often used in design of experiments. LHS works by sequentially choosing random points in multidimensional space but ensures that each new point does not share any of its coordinates with any of the previously generated points, which will alleviate the issue of clustering often observed with truly random data.

#### D. Radial Basis Function Surrogate Model

A radial basis function surrogate model was the first database technique explored. In model testing, some data from the training set is kept from the model and is then used as an input for verification of the model. The two databases span the same ranges, and so one database could be used as the training set, and the other as the verification set.

To ensure that the verification data was inside the training dataset, data near the edges of the range of verification database was excluded for verification. This would severely affect the uniform database, as the majority of its points were on the edge of the ranges.

As the solutions for each verification input data are known, the error in the reported solutions can be determined. Figures 31 and 32 show the histograms for the mean squared errors of the validation  $\sigma$ - $\varepsilon_p$  curves and the surrogate model output.

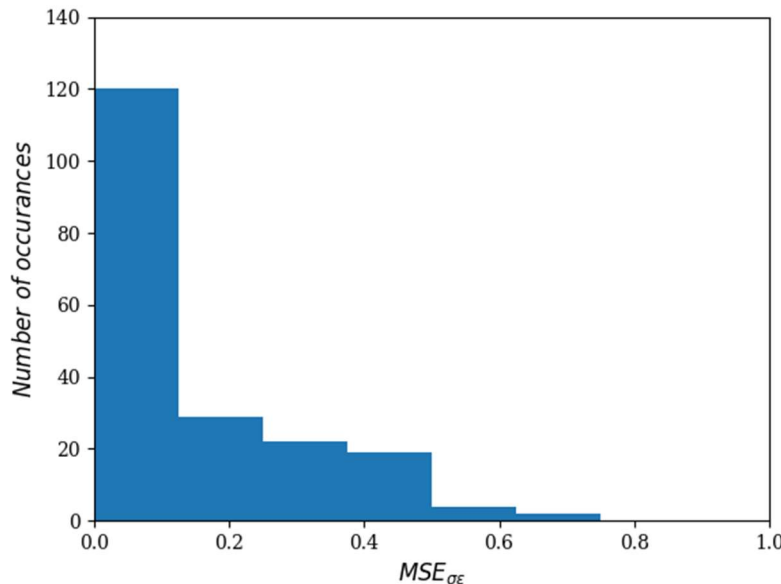


**Figure 31** MSE of  $\sigma$ - $\varepsilon_p$  curve for surrogate model estimation with uniform database

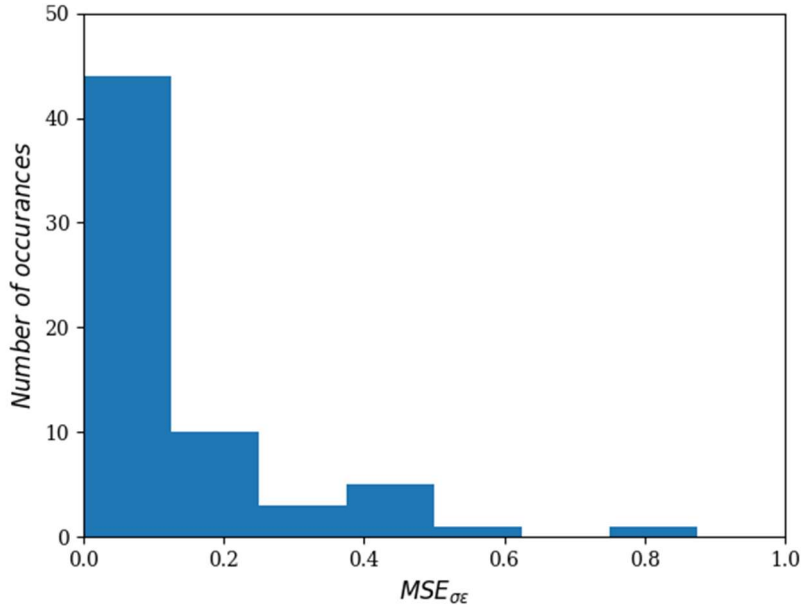


**Figure 32** MSE of  $\sigma$ - $\varepsilon_p$  curve for surrogate model estimation with LHS database

The surrogate model performed similarly regardless of if uniform or randomly spaced data was used for the training data.

Figures 33, 34, and 35 contain the best, mean, and 95<sup>th</sup> percentile estimated  $\sigma$ - $\varepsilon_p$  curves and their corresponding  $F$ - $h$  curves for the surrogate model. Figure 34 shows that the mean of the surrogate model estimation does reproduce a comparable  $\sigma$ - $\varepsilon_p$  curve, and Figure 35 shows that even the 95<sup>th</sup> percentile estimation of the  $\sigma$ - $\varepsilon_p$  curve still manages to very accurately reproduce the  $F$ - $h$  data.

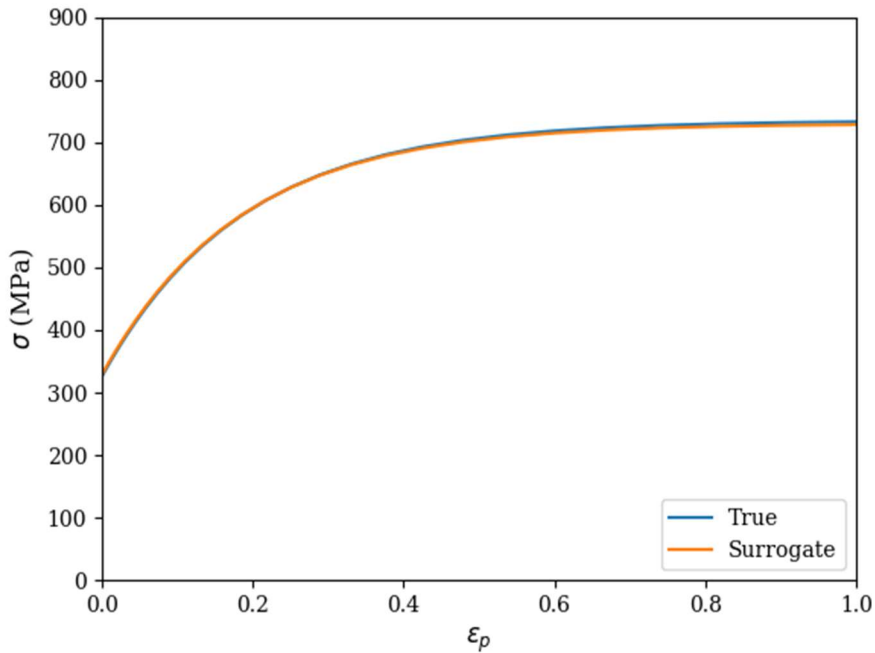


**Figure 33**  $\sigma$ - $\varepsilon_p$  curves for the best surrogate model estimation

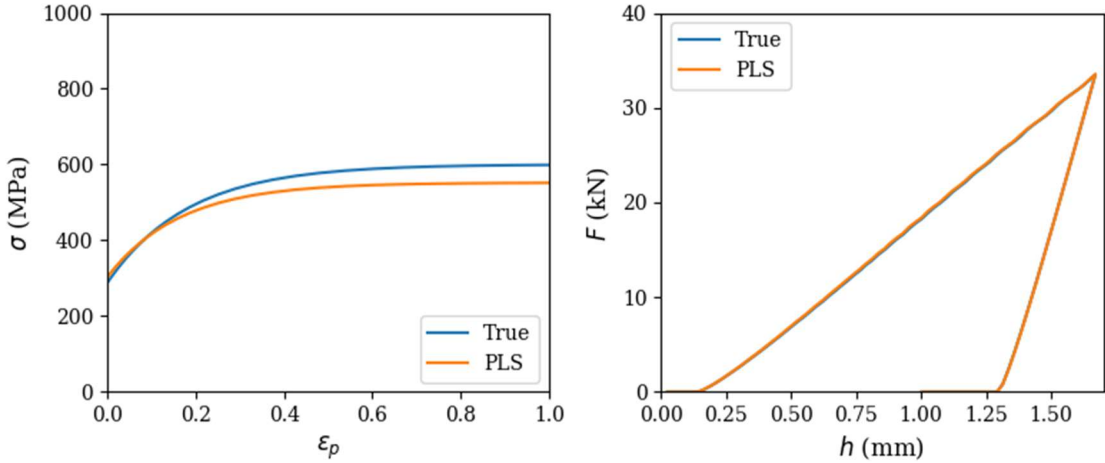


**Figure 34**  $\sigma$ - $\epsilon_p$  (left) and  $F$ - $h$  (right) curves for the mean surrogate model estimation

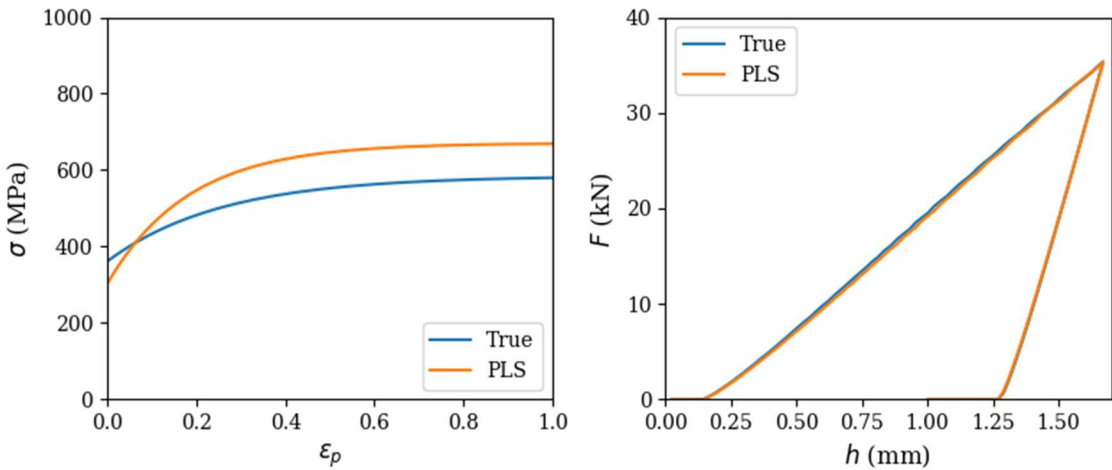


**Figure 35**  $\sigma$ - $\epsilon_p$  (left) and  $F$ - $h$  (right) curves for the 95<sup>th</sup> percentile surrogate model estimation

### 1. Presence of Family of Solutions

As the surrogate model is an approximation of the true  $F$ - $h$  error function, it is not computationally expensive to visually inspect the model if valleys are still present in the virtual problem compared to Figure 24 for the real problem. Figures 36, 37, and 38 show the contour plots of the surrogate model based on the centre data point. The contour plots show the mean squared error for the  $F$ - $h$  curve. For each contour plot, the fixed variable was set at the centre parameter, i.e. the parameter's true solution. By virtue of the model being an approximation of the virtual problem, the errors were not made relative to the any particular error.

A valley is clearly present in each figure regardless of the parameter being held constant. The valleys aren't seemingly very elongated ellipses, but rather distinct parabolic valleys, and as such a line of potential solutions will be present, or something akin to a rotated set of axis in the full three-dimensional space for all three parameters.

It can also be seen that the true solution for the problem is contained in these valleys, and so any model or error noise may unpredictably perturb the solution along these valleys.

All the valleys show that all the parameters can vary by 50% without a drastic change in the error of the  $F$ - $h$  curve. This shows that the virtual problem is ill-posed to a large degree.

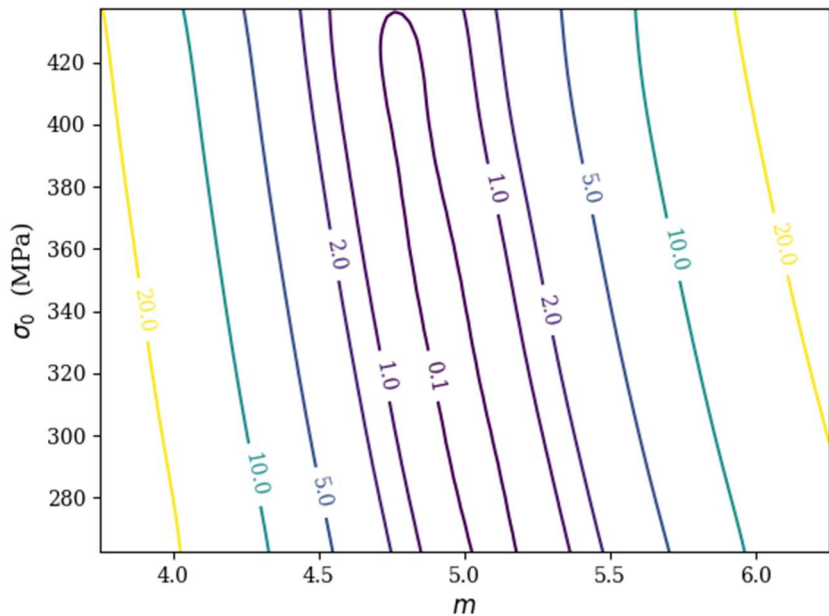


**Figure 36** Contour plot of the MSE for the F-h curve with fixed  $b$  parameter

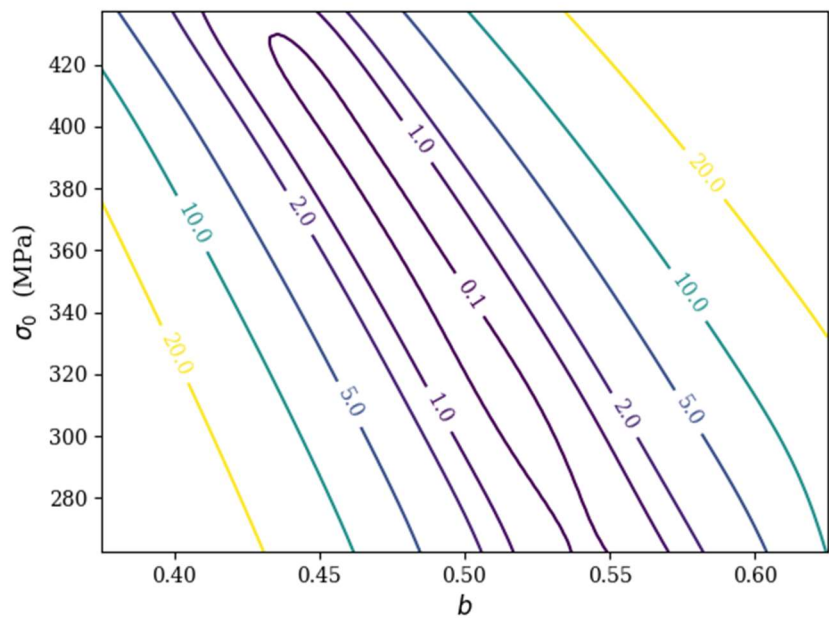


**Figure 37** Contour plot of the MSE for the F-h curve with fixed  $m$  parameter

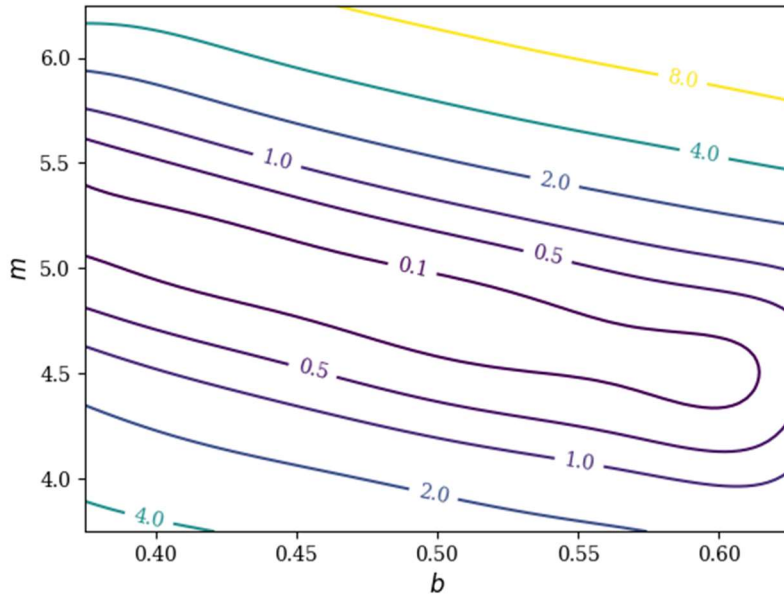


**Figure 38** Contour plot of the MSE for the  $F$ - $h$  curve with fixed  $\sigma_0$  parameter

### E. Statistical Regression

The second database technique explored was PLS. Only the uniform database was used for training the PLS regression as it would allow more validation data to be used. Based on the surrogate model the databases should not perform significantly differently.

The data to construct the dependent variable  $Y$  and dependent variable  $X$  for PLS regression should in the form given by equation (3.5), or to simplify

$$Y = XB. \quad (6.1)$$

Only the  $F$ - $h$  curve was used for the independent variable. To form the  $X$  matrix, the individual vectors,  $\mathbf{x}$ , are the reaction force of  $m$  points on the loading curve at a priori decided fixed displacements  $h_i$ , or

$$\mathbf{x} = [F_{h1} \quad F_{h2} \quad \cdots \quad F_{hm}]^T. \quad (6.2)$$

These vectors are stacked sequentially to form the matrix. As PLS does not factor what sort of relationship the independent variables share with each other, either the model parameters or the entire  $\sigma$ - $\varepsilon_p$  curve could be used as the dependent variable,  $Y$ , in equation (6.1). The parameters will form the vector

$$\mathbf{y} = [\sigma_0 \quad b \quad m]^T. \quad (6.3)$$

Alternatively, as with the  $F$ - $h$  curve, the  $\mathbf{y}$  vector could be the stress at  $p$  points at predetermined plastic strains. Both of these dependent variable forms were tested, and the mean squared error for the  $\sigma$ - $\varepsilon_p$  verification curves are shown in Figures 39 and 40 respectively. Note that the definition and calculation of the mean squared error is the same as that of the surrogate model, and thus can be numerically compared.

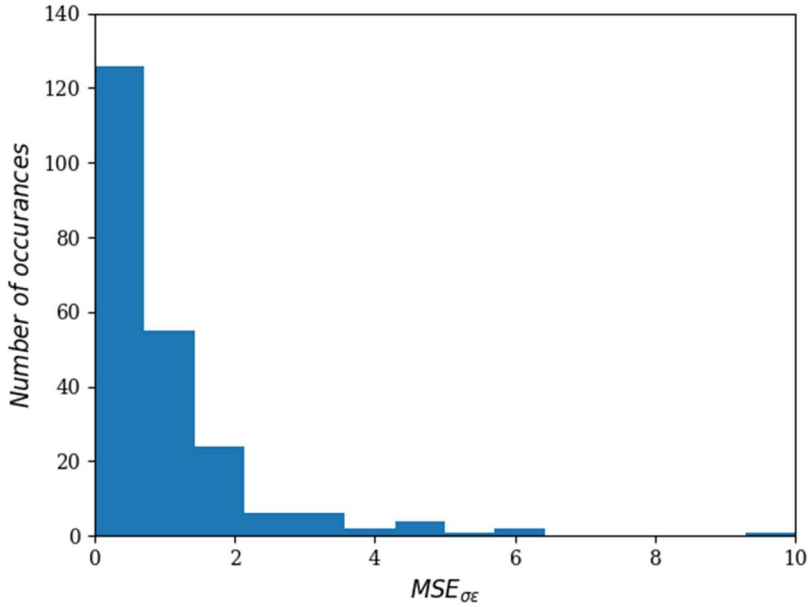


**Figure 39** MSE of  $\sigma$ - $\varepsilon_p$  curve for PLS using parameters

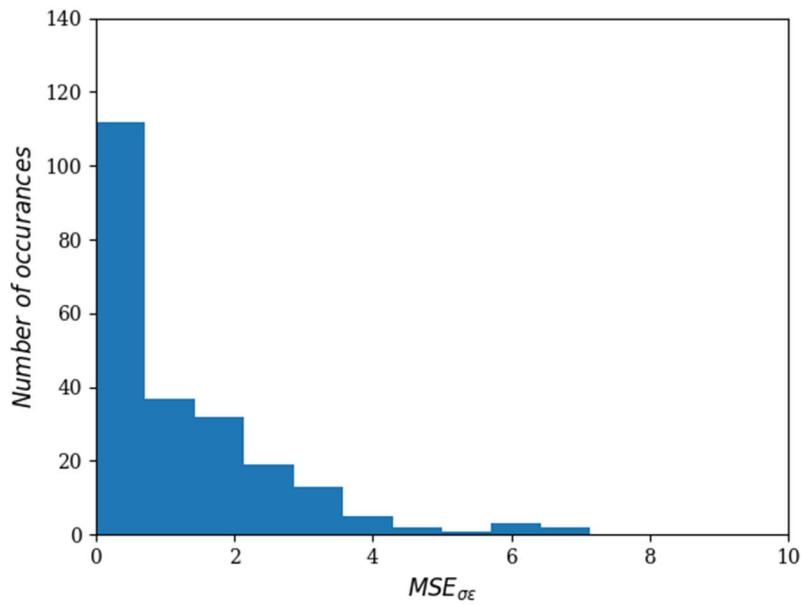


**Figure 40** MSE of  $\sigma$ - $\varepsilon_p$  curve for PLS using  $\sigma$ - $\varepsilon_p$  curves

It can be seen that using either the parameters or  $\sigma$ - $\varepsilon_p$  curves produce similar prediction distributions.

The best PLS was prediction was as accurate as the surrogate model and is not presented. Figures 41 and 42 show the mean and 95<sup>th</sup> percentile estimated  $\sigma$ - $\varepsilon_p$  curves and their corresponding  $F$ - $h$  curves for PLS using parameters. The figures also show the database mean curve, i.e. the curve described in Table 6.

For the surrogate model, the 95<sup>th</sup> percentile error was 0.45, but for PLS using either the parameters or  $\sigma$ - $\varepsilon_p$  curves the mean error is approximately 0.6. It can also be seen that the maximum error for the surrogate model is 0.8, while the maximum error using PLS is 10.

When considering Figures 34 and 42 for the surrogate model mean and PLS 95<sup>th</sup> percentile data respectively, it can be seen that the resultant  $F$ - $h$  curves are significantly different despite the roughly comparable  $\sigma$ - $\epsilon_p$  errors.

If the PLS results are accurate, it shows that PLS is not an appropriate statistical technique for this problem.

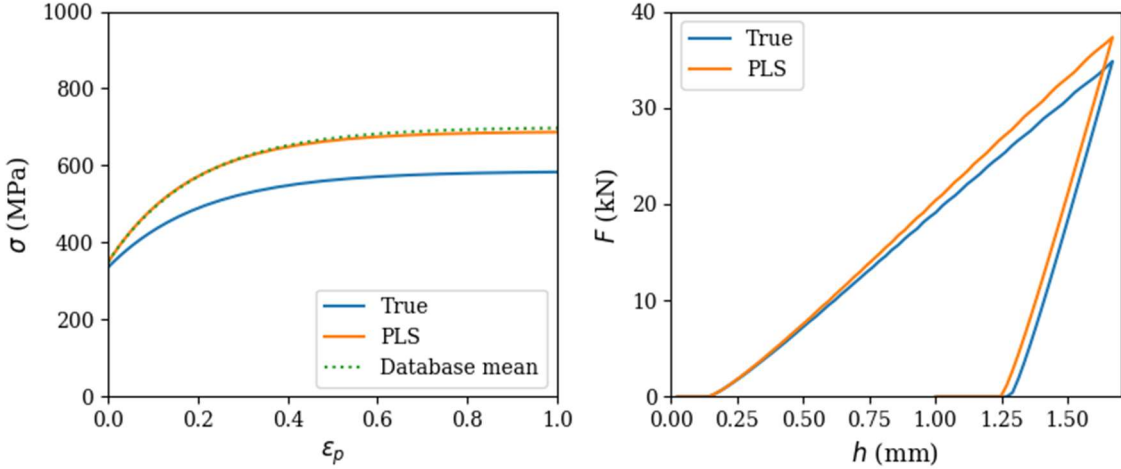


**Figure 41**  $\sigma$ - $\epsilon_p$  (left) and  $F$ - $h$  (right) curves for the mean PLS prediction

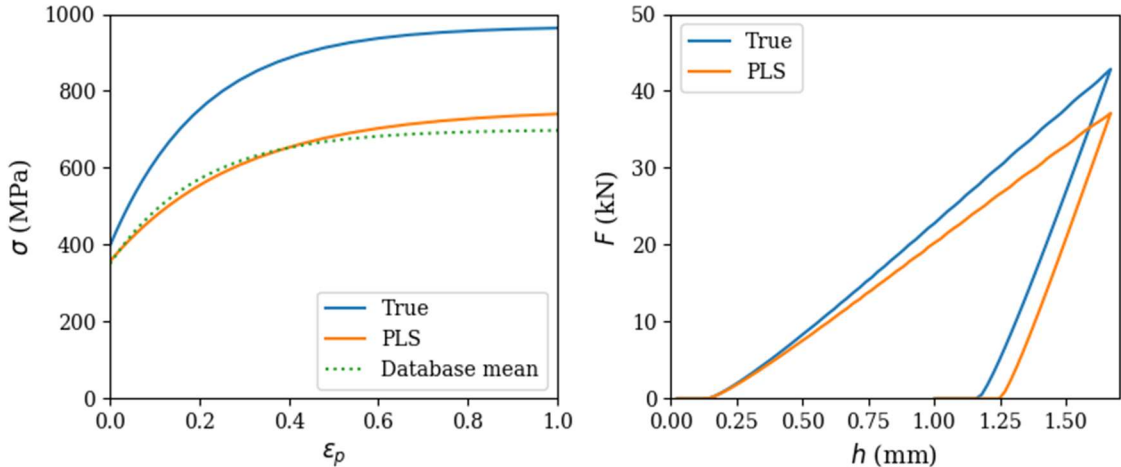


**Figure 42**  $\sigma$ - $\epsilon_p$  (left) and  $F$ - $h$  (right) curves for the 95<sup>th</sup> percentile PLS prediction

One thing which can be noticed is that for the mean and 95<sup>th</sup> percentile the predicted  $\sigma$ - $\epsilon_p$  curves were closer to the database mean than the true  $\sigma$ - $\epsilon_p$  curve.

The parameter based PLS predictions for the yield stress are shown in Figure 43, 44, and 45. It can be seen that the distributions are random, which is expected as the verification data is randomly distributed. However, the range that the yield stresses varies over is smaller than the training and verification databases ranges, as per Table 6. The saturation constant,  $b$ , also exhibits a much smaller range than Table 6 suggests the data should encompass. Conversely, the initial work hardening rate constant,  $m$ , would vary outside of the database range. This means that the lower and upper bounds of the  $\sigma$ - $\epsilon_p$  curve are essentially bounded by the yield and saturation stresses.

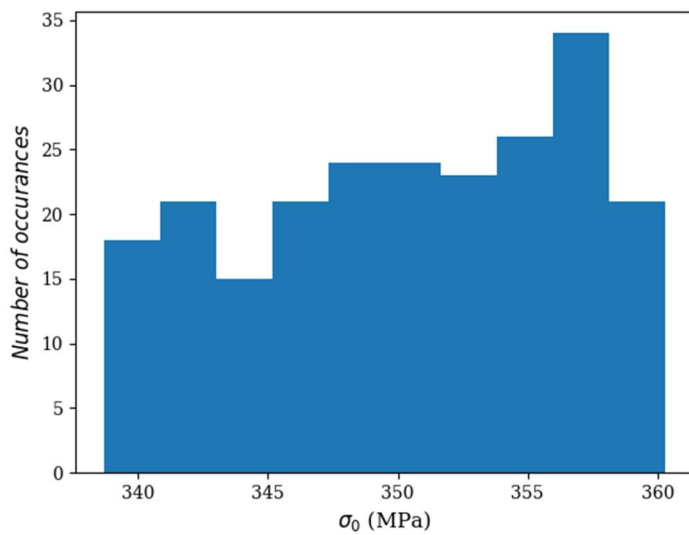


**Figure 43** PLS  $\sigma_0$  parameter predictions

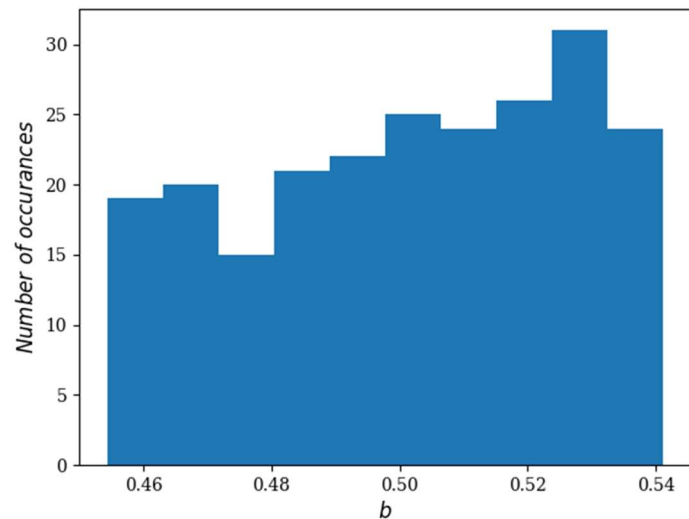


**Figure 44** PLS  $b$  parameter predictions

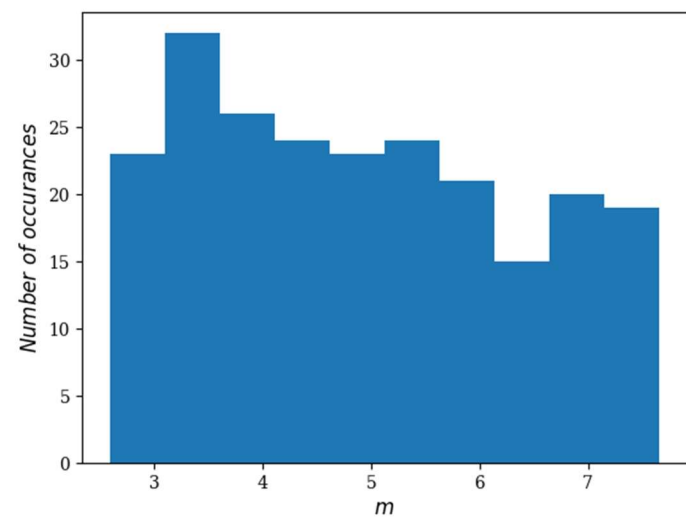


**Figure 45** PLS  $m$  parameter predictions

The lack of flexibility with which PLS could predict solutions explains the poor performance of the technique, as it would try to predict data with bounded data.

As the problem is ill-posed, it may influence the technique. Alternatively, the technique not working may be further evidence of the problem being ill-posed. PLS seeks to describe the variance in a dataset. For an ill-posed problem, one  $F$ - $h$  curve may relate to two very different  $\sigma$ - $\varepsilon_p$  curves, and will instead end up mapping to the average of these two  $\sigma$ - $\varepsilon_p$  curves which may be close to the mean curve. As such, it may predict very little variance from the mean, which is visible for two of the parameters as seen in Figure 43 and 44.

#### ***F. Analysis of Database Techniques***

The database techniques certainly had many improvements over direct optimisation. The databases could be built over the same amount of time it would take to do a single optimisation problem. The techniques could then be rapidly tested. The advantage of this is that the techniques may be statistically analysed as a large amount of data can quickly be gathered. This is not feasible for direct optimisation.

The surrogate model performed well, with the mean producing a similar  $\sigma$ - $\varepsilon_p$  curve to the solution and the 95<sup>th</sup> percentile estimation matching the  $F$ - $h$  data. Conversely, PLS could not accurately match the  $\sigma$ - $\varepsilon_p$  or  $F$ - $h$  curves. As the same database was used for both techniques, this could either suggest that PLS is not appropriate for this problem, or the technique was implemented incorrectly. In either case, further work can be done to find the reason behind the poor performance, and to investigate other statistical regression or machine learning techniques.

In terms of database distributions, both uniform and random distributions performed similarly.

Lastly, as the problem is ill-posed it is possible that for many of the instances where the  $\sigma$ - $\varepsilon_p$  estimation is poor, the techniques may still be able to produce an  $F$ - $h$  which matches the target  $F$ - $h$  curve. This is seen in the 95<sup>th</sup> percentile surrogate model estimation in Figure 35.

#### ***G. Uniqueness of Problem***

Evidence thus far points towards the virtual problem being ill-posed. The problem has been shown to be an ill-posed problem with the experimental data, but the virtual data shows that the problem itself is ill-posed. Even when minute errors are allowable, the solution is not unique, and the problem is therefore ill-posed.

To test the limits of a solution with reasonable errors, a new virtual optimisation problem was formulated. As the  $\sigma$ - $\varepsilon_p$  curve error is known for any curve in the virtual problem, it could be maximised in a general optimisation formulation

$$\min_x f(x) = \min_x (e^{(Fh)} + e^{(rh)} - e^{(\sigma\varepsilon)}). \quad (6.4)$$

This formulation is of a multi-objective optimisation problem, and would require analysing the Pareto efficiency of the solutions.

However, the formulation was not indented to rigorously explored, and as such the optimisation process was heuristically controlled to search for  $\sigma$ - $\varepsilon_p$  curves of interest. One such curve is presented here as the “worst-fit” curve. Figure 46 shows the worst-fit curve compared to its target curve, or “real” material.

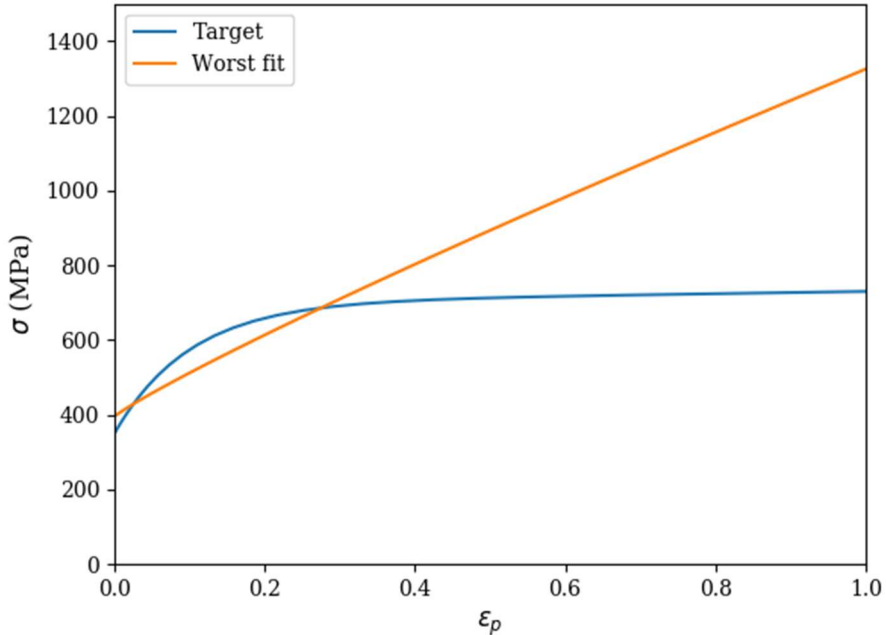


**Figure 46** Target and worst fit  $\sigma$ - $\varepsilon_p$  curves

Figure 47 shows the  $F$ - $h$  curves for the materials, and it can be seen that for any displacements below 1.4 mm the curves are similar, with minor deviations occurring at larger displacements. These displacements are however still potentially within a band of experimental error.

It can clearly be seen that despite wildly different plastic behaviours, saturating and nearly linear, the two  $\sigma$ - $\varepsilon_p$  curves produce similar  $F$ - $h$  curves. While the yield stresses have a difference of about 50 MPa, it is potentially more concerning that at a plastic strain of 0.6 the model would predict strains that can differ by approximately 350 MPa. This has major implications for large-deformation operations, such as metal forming or crumpling in safety structures, and will bring a multitude of issues into the reliability of using spherical indentation to determine the  $\sigma$ - $\varepsilon_p$  curve at large strains.

As such, it is necessary to try form additional tests which can more accurately differentiate between these two different curves.

### 1. Intermediate Surface Profiles

One method for possibly distinguishing between worst-fit and true materials found in the previous section is to observe the surface profile at different depths during loading. To facilitate this in a real experiment, several indentation tests can be done at different depths, and the surface profiles can be scanned. This was done numerically by running 3 different simulations that would have different final displacements. The three  $F$ - $h$  curves and surface profiles for both the target and worst fit curves can be seen in Figures 47 and 48 respectively.

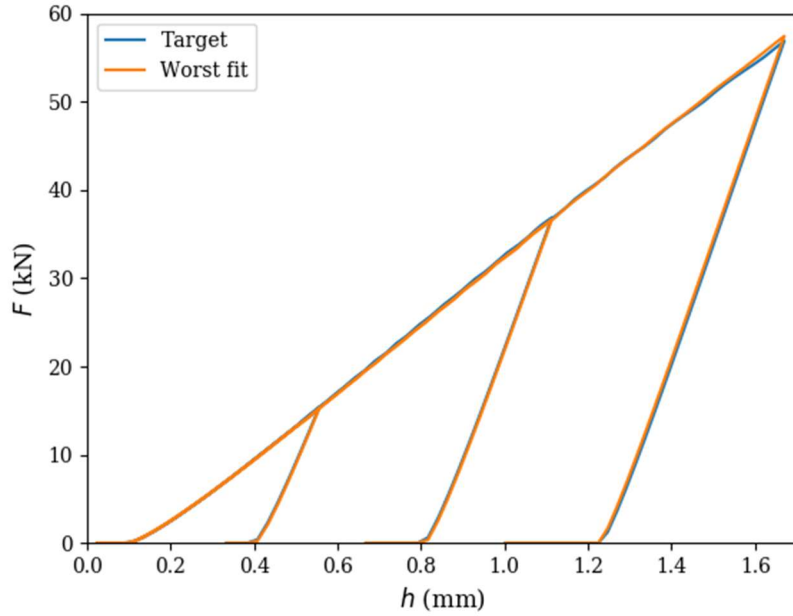


**Figure 47** Target and worst fit  $F$ - $h$  curves with multiple unloading steps

Figure 48 shows that all the surface profiles are essentially superimposed, which shows that scanning the surface profile at various depths is not a feasible way to distinguish between the two materials.

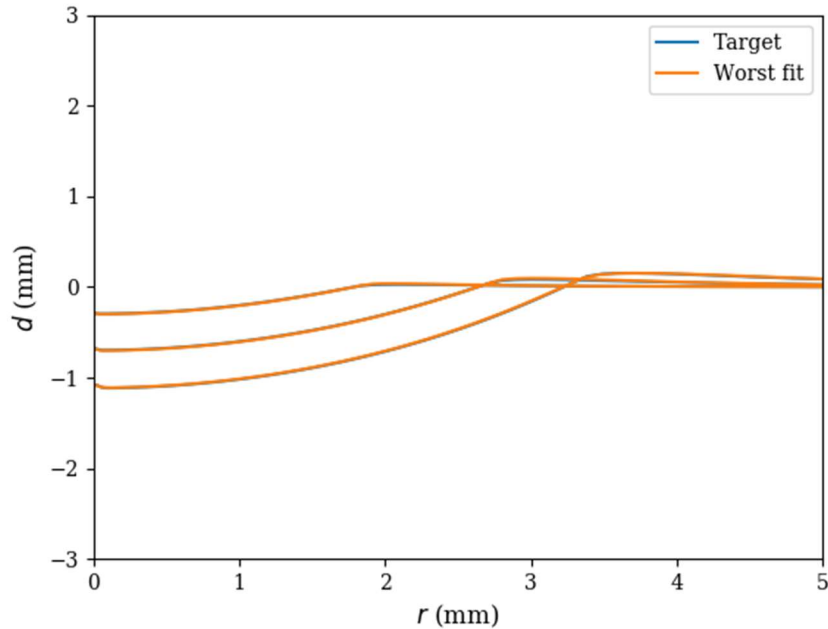


**Figure 48** Target and worst fit surface profiles with multiple unloading steps

## 2. Non-spherical Indenter

Another possible method for checking for uniqueness would be to use a different indenter shape. To investigate this, a non-rigid conical indenter was used. The conical indenter was also subjected to multiple unloading steps as with the spherical indenter.

Figures 49 and 50 shows the conical indenter was also not able to sufficiently distinguish between the two curves with regards to the  $F$ - $h$  curve or the surface profiles.

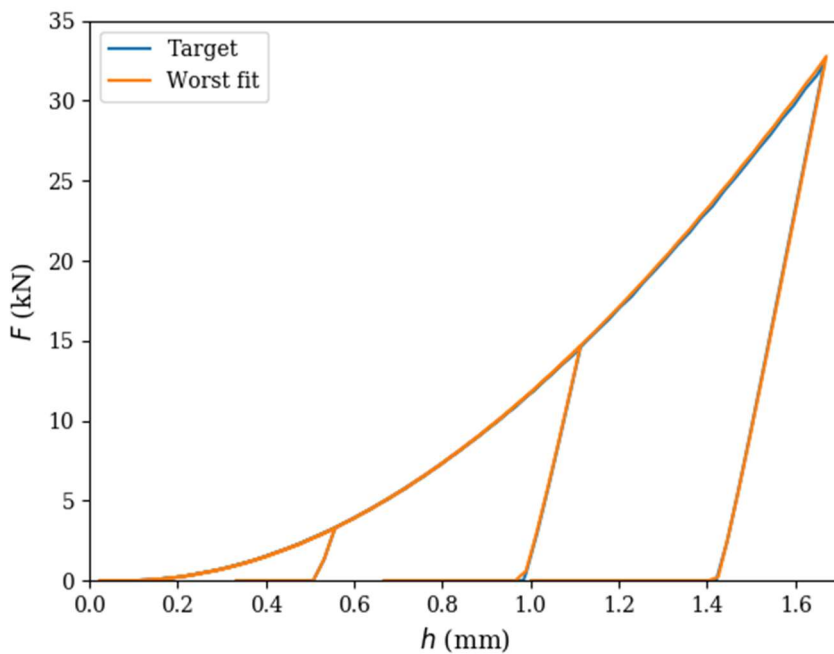


**Figure 49** Target and worst fit  $F$ - $h$  curves with multiple unloading steps

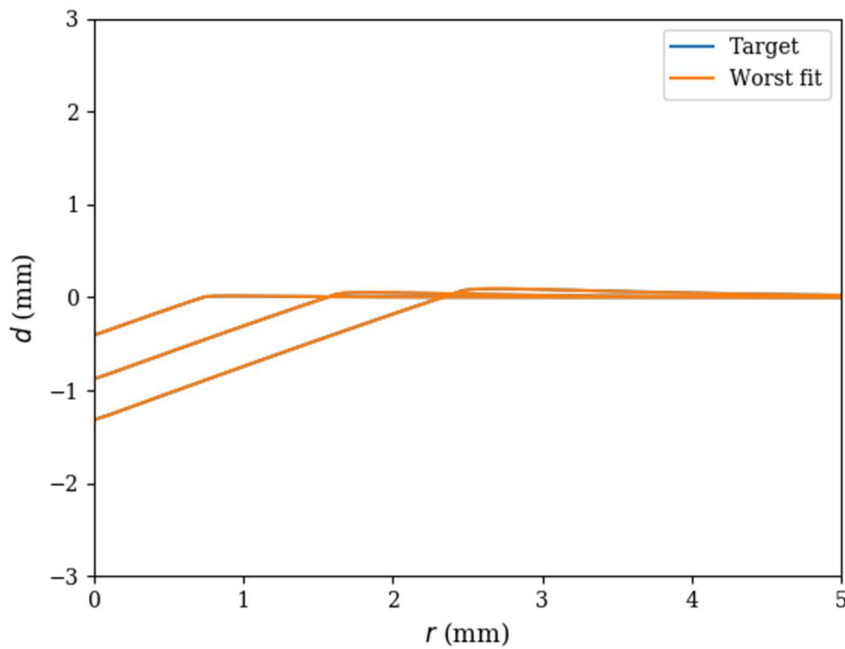


**Figure 50** Target and worst fit surface profiles with multiple unloading steps

Chen et al. (2007) found that with conical indenters at a variety of angles it was still possible to find a family of solutions which would result in a many-to-one correspondence between  $\sigma_{ep}$  and  $F$ - $h$  curves. Based on the observed results, it is also possible that a lack of uniqueness is present for all indenter geometries, as two very different geometries were used.

### 3. Source of Lack of Uniqueness

Many macroscopic effects of the indentation have not been able to distinguish between the two different  $\sigma$ - $\varepsilon_p$  curves. For a possible explanation, consider the plastic-deformation work done by the indenter during indentation:

$$W^p = \int F dh. \quad (6.5)$$

The work is performed over the loading and unloading, which, unless residual stresses are present in the material after the indentation, means no elastic work will remain in the material. The finite element model assumed to be an isotropic work hardening Von Mises material, and so the specific plastic-deformation work is given by Chakrabarty (2006) as

$$dW_s^p = \hat{\sigma} d\hat{\varepsilon}_p. \quad (6.6)$$

The total plastic-deformation work performed during the indentation is given by

$$\begin{aligned} W^p &= \int W_s^p dV \\ &= \iint \hat{\sigma} d\hat{\varepsilon}_p dV. \end{aligned} \quad (6.7)$$

To be a solution to the problem, the plastic deformation work will have to be a certain value as per equation (6.5). It is conceivable that the stress and plastic strain distributions may vary in equation (6.7) to allow for the integral to evaluate to the same value.

Figures 51 and 52 show the stress distribution for the target and worst-fit material at an indentation depth of 1.4 mm, where Figure 47 shows up that that displacement the  $F$ - $h$  curves are similar. Appendix H shows the equivalent plastic strain in the materials. It can be noted in Figures H1 and H2 that the plastic strains are largely identical, although this is expected as the problem is displacement prescribed.

As can be seen in Figure 52, the maximum stress is indeed higher for the worst-fit model, which corresponds to the  $\sigma$ - $\varepsilon_p$  curves in Figure 46. This confirms that the two materials are in fact distinguishable materials.

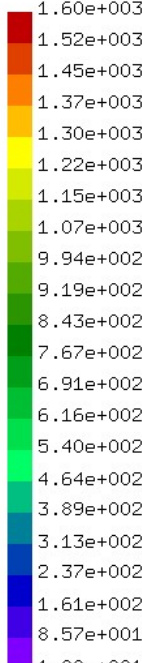
Also shown in Figure 52 are the contours for the stresses of the target material, which encompass larger volumes than the worst-fit material's equivalent stress contours. This supports the idea that while higher stresses are present for the worst-fit material, these stresses are concentrated in smaller volumes, and so when evaluating the integral in equation (6.6), the average stress among these materials are identical.

However, the mechanisms which cause the stress distributions to act as such are unknown. One method of investigating these mechanisms would be to analyse the stress distributions directly under the indenter instead. The stress distribution over the contact surface is given by

$$F = \int \sigma dA. \quad (6.8)$$

As the applied forces are constant between the two materials, they should have a certain value for the  $F$ - $h$  curves to match. The stress distributions in equation (6.8) may vary however. Analysing the pressure distribution on the contact surface may give insight into the stress distribution under the surface as well.

61/242:STRESS  
 Time:0.610000  
 Entity:Mises  
 +DispF:1.000000  
 max: 1.65e+003  
 min: 7.72e+000



Stress Value
1.60e+003
1.52e+003
1.45e+003
1.37e+003
1.30e+003
1.22e+003
1.15e+003
1.07e+003
9.94e+002
9.19e+002
8.43e+002
7.67e+002
6.91e+002
6.16e+002
5.40e+002
4.64e+002
3.89e+002
3.13e+002
2.37e+002
1.61e+002
8.57e+001
1.00e+001

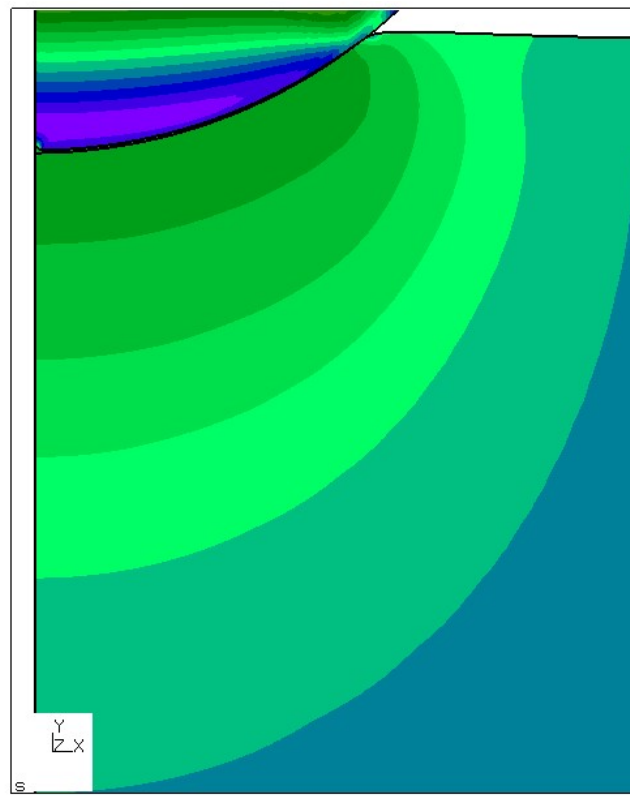
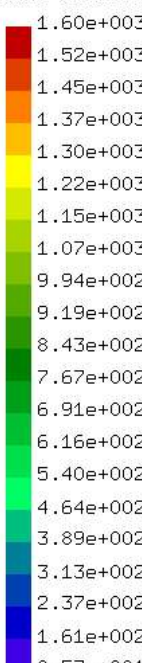


**Figure 51** Stress distribution in target material

61/242:STRESS  
 Time:0.610000  
 Entity:Mises  
 +DispF:1.000000  
 max: 1.66e+003  
 min: 3.25e+000



Stress Value
1.60e+003
1.52e+003
1.45e+003
1.37e+003
1.30e+003
1.22e+003
1.15e+003
1.07e+003
9.94e+002
9.19e+002
8.43e+002
7.67e+002
6.91e+002
6.16e+002
5.40e+002
4.64e+002
3.89e+002
3.13e+002
2.37e+002
1.61e+002
8.57e+001
1.00e+001

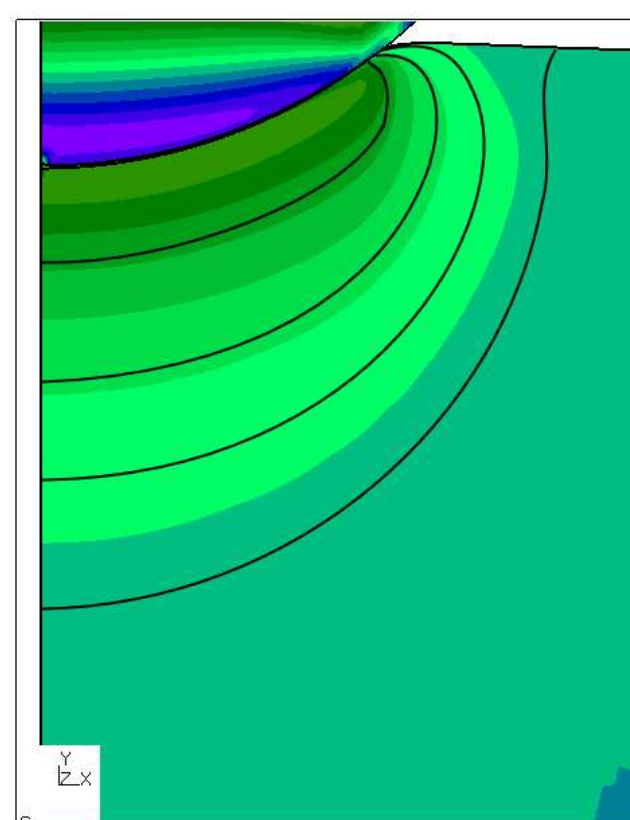


**Figure 52** Stress distribution in worst-fit material with target material stress contours

## VII. CONCLUSION

An indentation test was carried out, and a finite element model of the simulation was constructed. Furthermore, stress-strain curves were found which would match the forces in the experimental data. However, due to limitations in the finite element model, the surface profile could not be compared to that of the experimental surface profile. This was addressed by looking at a virtual problem's surface profile instead. As such, all the objectives for the research project were met.

Despite the project objectives being met, the research showed major difficulties in using an indentation test to determine the stress-strain curve of a material. When using experimental data, the choice of material model would result in different stress-strain curves. This was expected, but the behaviour of the stress-strain curves was not convergent as more flexibility was given to the models. This showed that the use of the experimental data was an ill-posed problem. Many examples of using an indentation test to determine material properties in literature were with micro-indentation on film layers. This could explain why contradictory results were found to the general view of the problem, as the dominant physics in the indentation may be scale dependent.

Causes for the lack of uniqueness may have included an incorrect friction model or plasticity in the indenter. The virtual problem would mitigate these issues, but unfortunately it could not impose uniqueness on the problem. Furthermore, by construction the finite element method is not scale dependent, and so the virtual problem is indicative of micro-indentation tests as well.

No practical techniques could be found which can distinguish between true and false solutions for the virtual problem, however it was seen that the two solutions are in fact indistinguishable. Furthermore,  $F$ - $h$  data alone appears to be fairly insensitive to any detail in the stress-strain curve as even the one model parameter model was able to match large portions of the  $F$ - $h$  curve despite being a limited model for practical applications.

However, as the results are contradictory to the current scientific community at large, the circumstances around the lack of uniqueness in the problem should be considered. It may possible that the specific problem investigated may not be unique, but due to error in either analysis or construction it is not representative of the problem which the majority authors have investigated. While the findings are not conclusive on the matter of general indentation tests, it certainly challenges the current assumption that the problem is generally well posed or that the uniqueness need not be investigated thoroughly.

For the material models, it was shown that the three parameter saturation based  $\sigma$ - $\varepsilon_p$  model was the simplest model which could extract as much information for the  $F$ - $h$  curve as possible. This is seen as it performed better than the one and two parameter models, and the four parameter model did not offer any improvements over the three parameter model. The three parameter model was also able to nearly exactly match the virtual  $F$ - $h$  curve for a stress-strain curve of a different mathematical form, but this attests to the lack of uniqueness in the problem rather than the abilities of the model. Lastly, it was also seen that while the three parameter model achieved the smallest error, even the one parameter model was able to match the  $F$ - $h$  curve to a degree despite being a poor model of true materials. This illustrates that the problem has either a lack of information which the  $F$ - $h$  can provide about the stress-strain curve, the lack on uniqueness in the problem, or both.

On the investigation of numerical methods for the problem, the conventional methods proved to be reliable, namely direct optimisation and a radial basis function surrogate model. Both methods would consistently match the  $F$ - $h$  data. However, due to a lack of uniqueness, the reported solution may not be the correct one. Additionally, these techniques appear to be resilient to the lack of uniqueness in the problem, i.e. being able to produce a result which can match the  $F$ - $h$  curve. Therefore, this shows that the techniques can illustrate a lack of uniqueness in a problem, but can also report accurate but false solutions. These techniques may not be applicable for problems where the solution is entirely unknown beforehand.

Conversely, partial least squares proved to be an ineffective method for this problem. This could be due to the fact that the problem is ill-posed or the algorithm was implemented incorrectly, but these possibilities were not investigated rigorously, and so future work can be done on it. However, the fact that PLS could not produce accurate results could be advantageous. PLS did not return false solutions, as the solutions it produced were easy to verify as being incorrect. This means that PLS could be less likely to produce false if the results aren't scrutinised. Based on these factors, no strong conclusions about PLS may be drawn for this problem in particular.

Lastly, the database techniques showed major advantages over conventional optimisation. In the time one optimisation procedure could be done, an entire database could be built and tested, and successive curves could be rapidly analysed thereafter. Furthermore, the database techniques allowed two different identification techniques to be tested on the same set of data, which helps to verify the solution obtained by either.

In summary, the research showed that it is in fact possible to solve the problem of determining the stress-strain curve of a material from an indentation test. However, the research also showed that the results are not unique, thereby challenging the assumption of uniqueness in the problem.

### ***Recommendations***

The first and foremost recommendation of further work would be to investigate the lack of uniqueness in the solutions. To confirm the lack of uniqueness, the FEM model should be verified to be correct, and results should be reproduced to ensure their validity.

Should the problem still be shown to be ill-posed, there are two proposed paths which could follow to investigate the uniqueness of the problem are:

1. To investigate techniques which could distinguish false solutions of the problem.
2. To investigate the fundamental cause of the lack of uniqueness in the problem.

One possible experiment that could encompass both of these paths would be to perform an indentation test and capture the stress distribution at the contact surface. This could be accomplished numerically or experimentally with the use of a piezoelectric indenter.

Despite the lack of success with machine learning, further work can be done on its application to structural mechanics' problems. This can include investigating the poor performance of PLS on the problem, or investigating other forms of machine learning on the problem, such as artificial neural networks. Alternatively, different structural mechanics problems may be investigated using machine learning compared to conventional techniques.

## REFERENCES

- Beghini, M., Bertini, L. & Fontanari, V., 2006. Evaluation of the stress-strain curve of metallic materials by spherical indentation. *International Journal of Solids and Structures*, Volume 43, pp. 1442-2459.
- Chakrabarty, J., 2006. *Theory of Plasticity*. 3rd ed. Burlington: Elsevier Butterworth-Heinemann.
- Chen, X., Ogasawara, N., Zhao, M. & Chiba, N., 2007. On the uniqueness of measuring elastoplastic. *Journal of the Mechanics and Physics of Solids*, Volume 55, p. 1618–1660.
- Dhondt, G., 2016. *CalculiX CrunchiX USER'S MANUAL version*.
- Downling, N., 1999. *Mechanical Behaviour of Materials*. 2nd ed. New Jersey: Prentice Hall.
- Gao, X., Zhang, T., Hayden, H. & Roe, C., 2009. Effects of the stress state on plasticity and ductile failure of an aluminium 5083 alloy. *International Journal of Plasticity*, Volume 25, pp. 2366-2382.
- Geladi, P. & Kowalski, B., 1986. Partial Least-Squares Regression: A Tutorial. *Analytica Chimica Acta*, Volume 185, pp. 1-17.
- Gelin, J. & Ghouti, O., 1996. An inverse solution procedure for material parameters identification in large plastic deformation. *Communications in Numerical Methods in Engineering*, Volume 12, pp. 161-173.
- Hadamard, J., 1902. Sur les problèmes aux dérivées partielles et leur signification physique. *Princeton University Bulletin*, pp. 49-52.
- Huber, N., Munz, D. & Tsakmakis, C., 1997. Determination of Young's modulus by spherical indentation. *Journal of Materials Research*, 12(9), pp. 2459-2469.
- Jones, E., Oliphant, E., Peterson, P. & Others, 2001. *SciPy: Open Source Scientific Tools for Python*. [Online] Available at: <http://www.scipy.org/> [Accessed 06 09 2017].
- Kang, J., Becker, A. & Sun, W., 2011. A combined dimensional analysis and optimization approach for determining elastic-plastic properties from indentation tests. *Journal of Strain Analysis*, pp. 749-759.
- Kucharski, S. & Mroz, Z., 2007. Identification of yield stress and plastic hardening parameters. *International Journal of Mechanical Sciences*, Volume 49, p. 1238–1250.
- Laursen, T. & Simo, J., 1992. A study of the mechanics of microindentation using finite elements. *Journal of Materials Research*, 7(3), pp. 618-626.
- Mackerle, J., 2001. Finite element and boundary element simulations of indentation problems A bibliography (1997-2000). *Finite Elements in Analysis and Design*, Volume 37, pp. 811-819.
- Nelder, J. & Mead, R., 1965. A simplex method for function minimization. *The Computer Journal*, 7(4), pp. 308-313.

Norbury, A. & Samuel, T., 1928. The recovery and sinking-in or piling-up of material in the Brinell test, and the effects of these factors on the correlation of the Brinell with certain other hardness tests. *Iron Steel Inst.*, Volume 117, pp. 673-687.

Oliver, W. & Pharr, G., 1992. An improved technique for determining hardness and elastic modulus using load and displacement sensing indentation experiments. *Journal of Materials Research*, 7(6), pp. 1564-1583.

Pedregosa, F. et al., 2011. Scikit-learn: Machine Learning in Python. *JMLR*, Volume 12, pp. 2825-2830.

Savitzky, A. & Golay, M., 1964. Smoothing and Differentiation of Data by Simplified Least Squares Procedures. *Analytical Chemistry*, 36(8), pp. 1627-1639.

Snyman, J. & Wilke, D., 2017. *Practical Mathematical Optimisation*. 2nd ed. To Be Published.

Sung, J., Kim, J. & W. R., 2010. A plastic constitutive equation incorporating strain, strain-rate, and temperature. *International Journal of Plasticity*, 26(12), pp. 1746-1771.

Swain, M., 1993. A Simple Predictive Model for Spherical Indentation. *Journal of Materials Research*, 8(2), pp. 296-306.

Tabor, B., 1951. *The Hardness of Materials*. Oxford: Clarendon Press.

Taljat, B., Zacharia, T. & Kosel, F., 1998. New analytical procedure to determine stress-strain curve from spherical indentation data. *International Journal of Solid Structures*, 35(33), pp. 4411-4426.

Tulyukovskiy, E. & Huber, N., 2006. Identification of viscoplastic material parameters from spherical indentation data: Part I. Neural networks. *Journal of Materials Research*, 21(3), pp. 664-676.

Voce, E., 1948. The relationship between stress and strain for homogeneous deformation. *Journal of the Institute of Metals*, Volume 74, pp. 537-562.

Wang, H. et al., 2016. Surrogate-assisted Bayesian inverse material identification method and application to advanced high strength steel. *Inverse Problems in Science and Engineering*, 24(7), pp. 1133-1161.

## APPENDIX A: MEETING LOG CARD

### RESEARCH PROJECT – MRN 422

#### MEETING LOG CARD

Student Nick Kossolapov Student. no. 14344042

Research project Determine the stress-strain curve of aluminium using an indentation test

Date	Student signature	Supervisor signature	Comments
27/07	N.K	S.Ibl	
03/08	N.K	S.Ibl	
10/08	N.K	S.Ibl	
17/08	N.K	S.Ibl	
31/08	N.K	S.Ibl	
07/09	N.K	S.Ibl	
14/09	N.K	S.Ibl	
21/09	N.K	S.Ibl	

**APPENDIX B: RESEARCH PROJECT PROPOSAL**

**Determine the stress-strain curve of aluminium  
using an indentation test**

**Nick Kossolapov**

**14344042**

**MRN 412/422 Research Project Proposal**

## **1. Introduction**

With existing equipment in use, it is often necessary to be able to determine the material properties of the equipment. However, as the equipment is in use, non-destructive methods are to be used. Once such method is the micro-indentation test in order to obtain the applied force versus deflection curve of the material. The material properties can then be extracted from this data. This project is about the process of performing an indentation test, and then being able to extract, verify, and validate the material properties of a chosen specimen.

## **2. Problem statement**

The stress-strain curve of aluminium is to be obtained with an indentation test. However, an indentation test alone may not yield the true stress strain curve of a material by itself. One such method to obtain a more accurate stress-strain curve is to perform a reverse identification analysis using finite element analysis to match the results obtained by the indentation test.

## **3. Objectives**

There are 3 main goals associated with this project, namely:

1. To plan, setup, and perform an indentation test.
2. To simulate the problem using finite element software.
3. To modify the simulation to match both the forces in the experiment as well as the deformation geometries.

## **4. Scope**

The aspects of the problem which need to be understood include indentation tests, plastic deformation, the finite element method for plastic deformation, as well as inverse problems for material identification. Firstly, a literature study will be done on these topics.

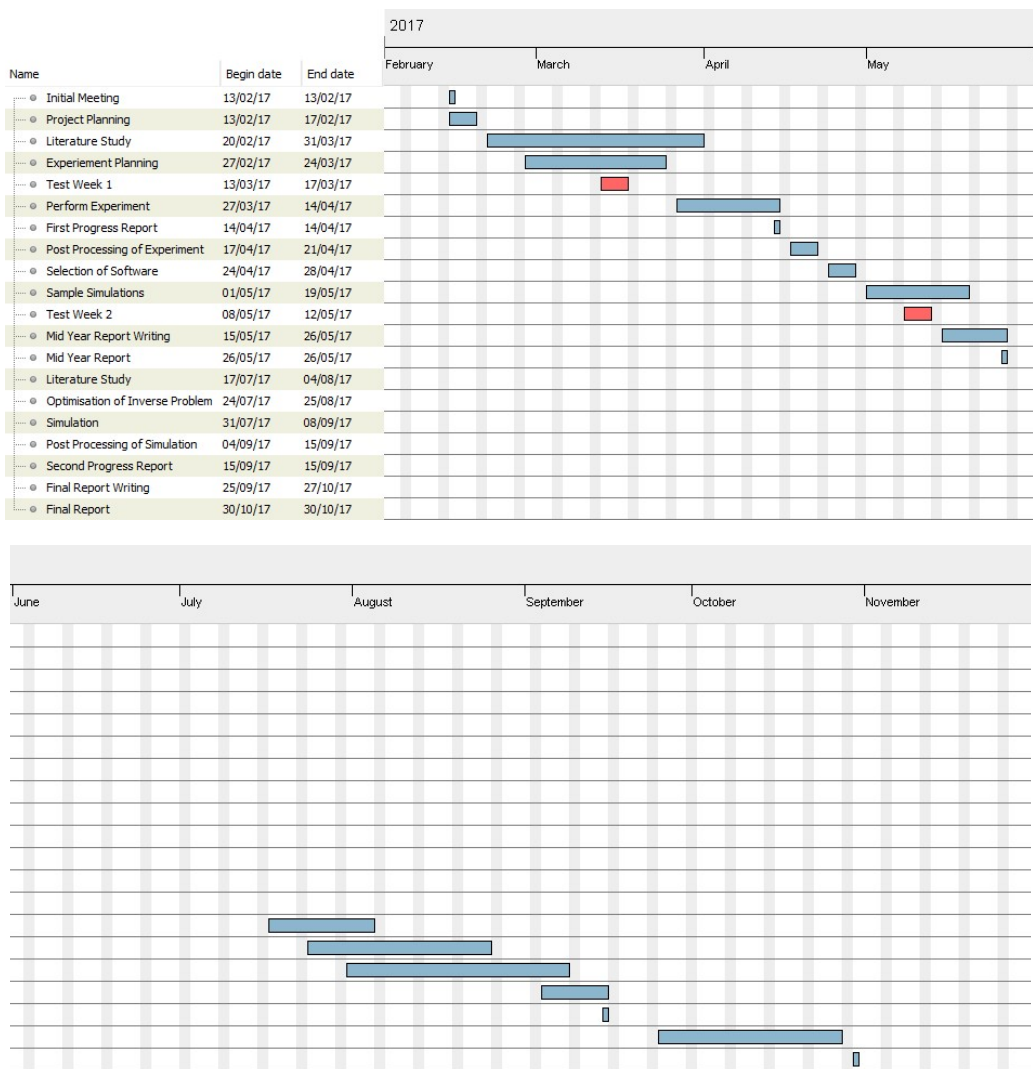
An indentation test will have to be designed, planned, and carried out. In the indentation test, the applied force versus deflection as well as the final geometry of the indentation will be recorded.

For the simulation of the problem, a software solution and optimisation technique will have to be selected, calibrated, and possibly scripted in order to handle the reverse identification problem. A method will have to be established in order to compare the simulated results to the experiment. The results will also need to be verified and validated.

## **5. Deliverables**

The projects main deliverable will be a report detailing the work undertaken, conclusions drawn, and possible recommendations.

Other deliverables will include an experimental setup which can perform an indentation test, and an oral presentation and poster exhibition of the project.



## Project Proposal Compliance Matrix

Requirement	Proposal		Project Report	
	Section	Page	Section	Page
Plan, setup, and perform an indentation test.	2	1	III.A	7
Record the applied force versus deflection as well as the final geometry of the indentation.	3	1	III.B	8
Simulate the problem using finite element software.	2	1	IV.B	10
Select an optimisation technique.	3	1	IV.E	16
To modify the simulation to match both the forces in the experiment as well as the deformation geometries.	2	1	V	18-23
Compare the simulated results to the experimental results.	3	1	V	18-23
Verify and validate the results	3	1	VI	31-48
Discuss results and draw conclusions	5	1	VII	49-50
Make recommendations for future improvements	5	1	VII	50

## **APPENDIX C: PROGRESS REPORTS**

Progress Report – 20 April 2017

### ***A. Work Completed to Date***

The current tasks identified in the progress report which have been completed are

- Literature study
- Experiment planning
- Experiment
- Post-processing of results
- Selection of software.

However, further experiments have been planned for the second semester, and literature study is an ongoing process alongside normal work.

### ***B. Project Plan***

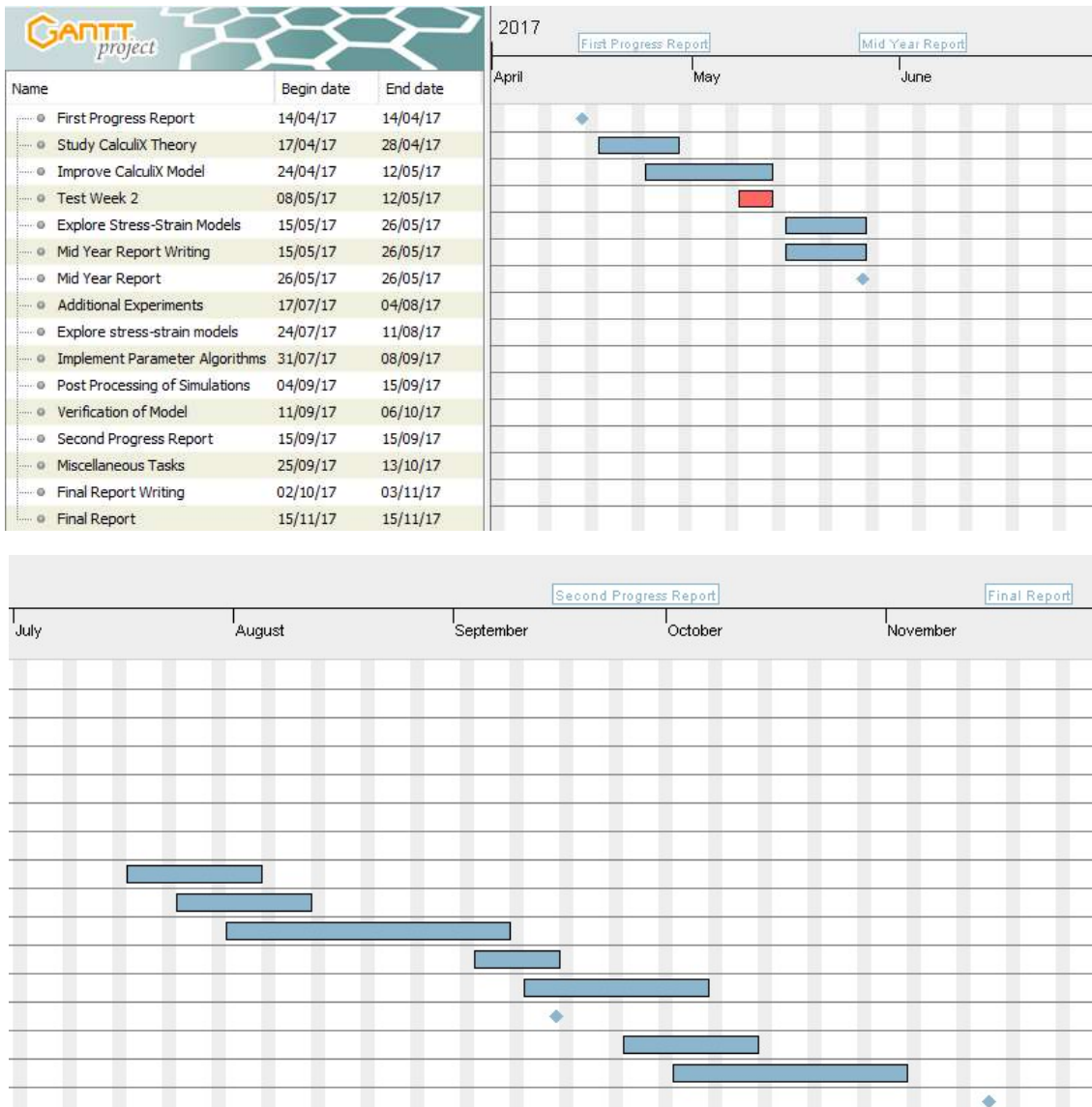
An updated project plan is shown on the following page.

Note that this project plan still excludes work during the June/July holidays. This is merely a precautionary measure, as reasons outside of my control could prevent me from working continuously during the period.

### ***C. Personal Opinion***

I feel that the project is progressing well. While the current work feels insufficient, notably the experiment, the steady progress allows identification of where work needs to be done.

While I have found a sufficient amount of literature on the topic, as it is beyond the scope of an undergraduate course, more time is needed to properly read and digest the information in the papers and articles. Therefore, the current literature study of the report will need more work.



## Progress Report – 15 September 2017

### ***A. Work Completed to Date***

So far, the majority of the work for the second semester has been completed as per the first semester's project plan. The tasks completed this semester include:

- A direct optimisation environment was successfully made and used.
- Higher order material models were explored.
- Various factors that influence the FEM model were explored.
- The experimental data was matched, and uniqueness of the solution has been partially explored.
- The project was moved to a virtual problem.
- The influence of the surface profile on direct optimisation was explored.
- The databases were formed, and the surrogate models and machine learning algorithms were chosen and have been implemented.

### ***B. Project Plan***

Currently, work is being done on analysing the surrogate models and machine learning algorithms. Several inconsistencies have been found with the data, and is being explored. The already presented data is also being checked.

After these issues have been dealt with, the effect of noise on the system will be explored. This noise will take the form of stochastic noise, and noise that modified the shape of the curve.

Lastly, if time permits, a brief investigation will be done on ways to potentially make the virtual problem well-posed, or at least unique. This includes briefly testing other indenter shapes, and getting the surface profile at varying stages of unloading.

### ***C. Personal Opinion***

The project is approaching completion. It looks to be possible to complete the project by the end of September, which will give me a month to go over the work and make any improvements.

I feel satisfied with the work done to date, however there is still much more work that can be done which likely won't be possible within time.

## APPENDIX D: CALCULIX INPUT FILES

### *GraphiX Script*

```
#adapted from hertz_axi by Martin Kraska
#[github.com/mkraska/CalculiX-Examples/tree/master/Contact/Hertz_axi]

valu radius 5
valu height 24
valu width 20

seto sphere
pnt p1 0 radius 0
pnt p2 0 0 0
pnt p3 radius radius 0
line peri p2 p3 p1 60 1.05
line l1 p2 p1 40 1.05
line l2 p3 p1 20 1
surf s1 l2 peri l1
move all tra 0 0.1 0
setc sphere
seto block
pnt p4 0 0 0
valu neg -1
valu neg_height * neg height
swept block block tra 0 neg_height 0 40
bia block 32
swept block block tra width 0 0 120
seta lb 1 L003 L004
bia block 64
#move block tra 1e-3 0 0
setc block
seto press
seta press 1 L004
swept press press tra 0 -5 0 1
flip press
move all tra 0 height 0
flip all
elty all qu4c
mesh all
send all abq
send sphere abq nam
send block abq nam
send press abq nam
rot -z
view elem
frame
seta speri 1 peri
comp speri do
comp speri do
send speri abq sur
send speri abq nam
seta sblk 1 L003
comp sblk do
comp sblk do
send sblk abq sur
seta x0 1 L001 l1 L006
comp x0 do
comp x0 do
send x0 abq nam
seta y0 1 L005
comp y0 do
comp y0 do
send y0 abq nam
seta control 1 12
comp control do
comp control do
```

```

send control abq nam
seta surface 1 L003
comp surface do
comp surface do
send surface abq nam

```

### ***CalculiX Input File***

All words preceded by a \$ serve as template placeholders for Python String templates, e.g. \$plastic serves as a placeholder for the plastic stress-strain data points.

```

*INCLUDE, input=all.msh
*INCLUDE, input=sblk.sur
*INCLUDE, input=speri.sur
*INCLUDE, input=x0.nam
*INCLUDE, input=y0.nam
*INCLUDE, input=block.nam
*INCLUDE, input=sphere.nam
*INCLUDE, input=press.nam
*INCLUDE, input=control.nam
*INCLUDE, input=surface.nam

*BOUNDARY
Nx0,1,,0
Ny0,2,,0
*MATERIAL,NAME=steel
*ELASTIC
2.1e5,0.3
*MATERIAL,NAME=press
*ELASTIC
$press_stiffness,0.0
*MATERIAL, NAME=aluminium
*ELASTIC
7e4,0.33
*PLASTIC
$plastic
*SOLID SECTION, ELSET=Esphere, MATERIAL=steel
*SOLID SECTION, ELSET=Epress, MATERIAL=press
*SOLID SECTION, ELSET=EBLOCK, MATERIAL=aluminium
*SURFACE INTERACTION, NAME=contact
*SURFACE BEHAVIOR, PRESSURE-OVERCLOSURE=linear
$spring_constant
$friction
*CONTACT PAIR, INTERACTION=contact, TYPE=SURFACE TO SURFACE
Ssblk, Ssperi
*AMPLITUDE, NAME=A1
0.0, 0.0, $mid_time, 1.0, 1.0, $end_disp
*STEP, NLGEOM, INC=5000
*STATIC
0.01, 1, 0.001, 0.01
*BOUNDARY, AMPLITUDE=A1
NControl, 2, 2, $amplitude
*NODE FILE, OUTPUT=2D
U
*EL FILE
S, E, PEEQ
*NODE PRINT, NSET=NControl, totals=only
RF
*NODE PRINT, OUTPUT=2D, NSET=NSurface
U
*END STEP

```

## APPENDIX E: UNIAXIAL TEST DATA

After an indentation test was performed, each of the six samples used were parted at a distance where the cut-off would not be within the plastic affected region, as obtained from the FEM simulation after the experimental data was matched.

Three sample's cut-off's were used in pure compression, and it shown in Figure E1. The  $F\text{-}h$  from the compression test was such that the elastic modulus of the  $F\text{-}h$  curve was that of the elastic modulus of aluminium. The elastic component of the curve was removed to produce the  $\sigma\text{-}\varepsilon_p$  curves as can be seen in Figure E1. The curves all have similar shapes, but vastly different yield stresses. The cause for this is unknown, and it likely equipment error.

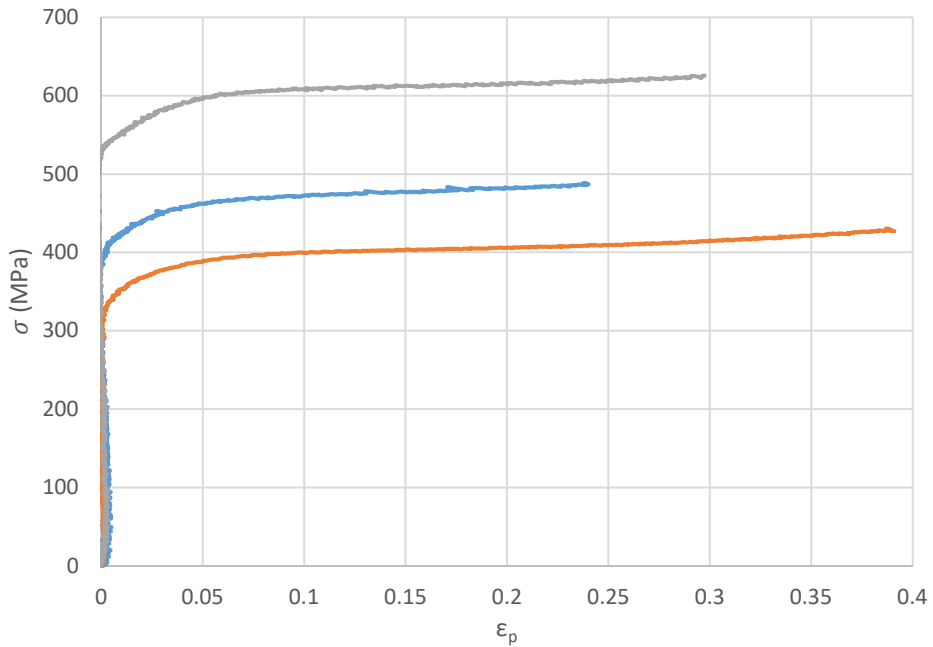


**Figure E1** Pure compression test data

The remaining three cut-offs were split into two tensile test specimens, or six samples in total. A standard tensile test was performed on each of these, with a sample  $F\text{-}h$  shown in Figure E2. The  $F\text{-}h$  curve in Figure E2 is not shaped like a typical tensile test curve. Therefore, the results cannot be trusted. The cause of this is unknown, and is again likely due to machine error.

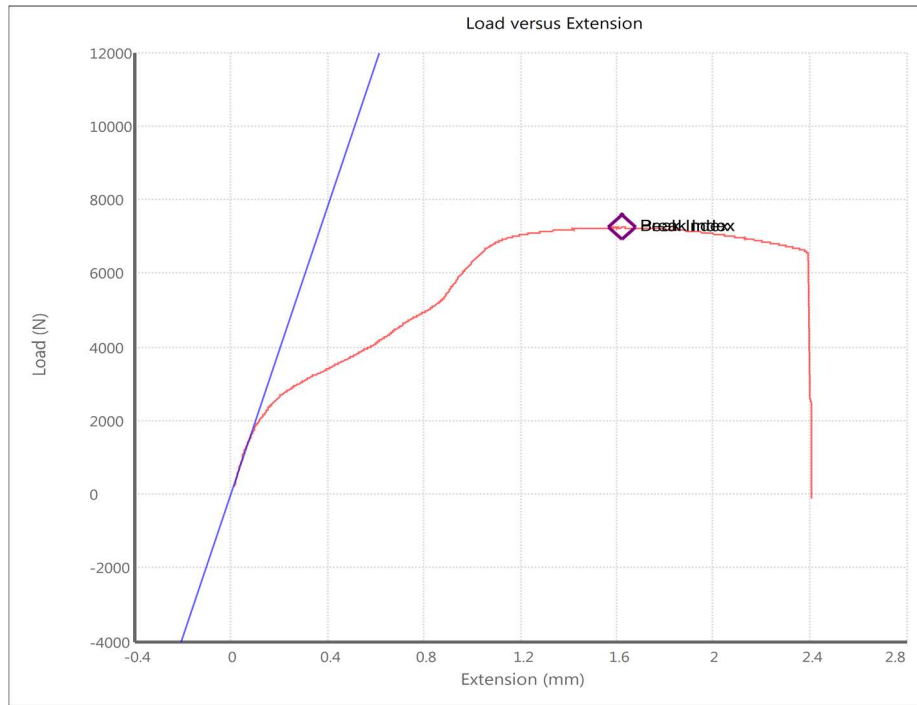


**Figure E2** Sample tensile data

Figure E3 shows the obtained plastic curves for each of the material models. It can be seen that the one parameter model best represents the pure compression test data despite being the worst fit. This shows that the experimental cannot be used.

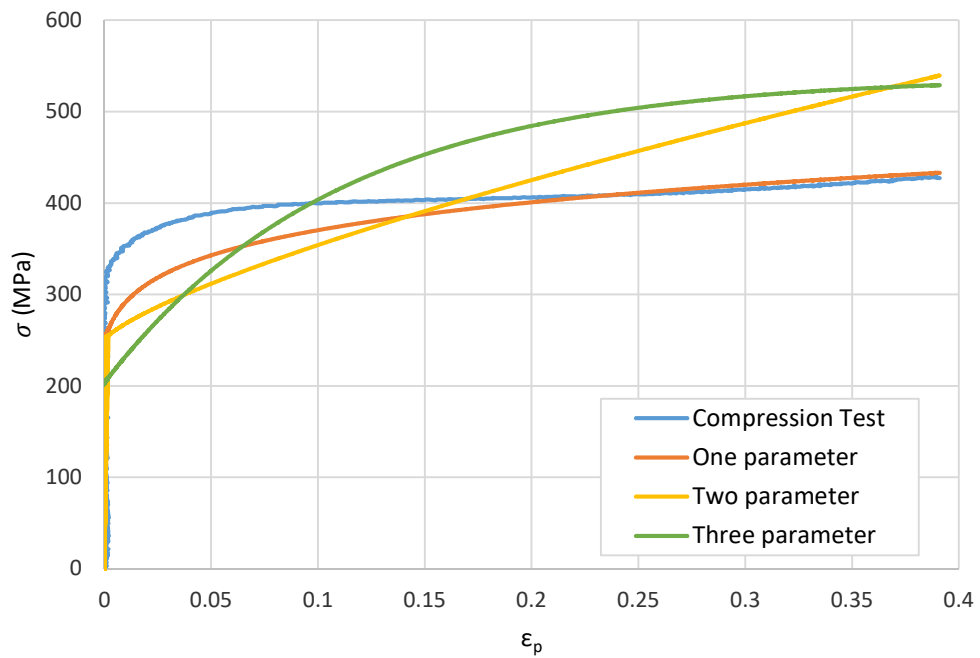


**Figure E3** Plastic curves for models and experimental data

## APPENDIX F: DATABASE TECHNIQUES

### *Radial Basis Function*

Surrogate models seek to approximate the function by considering the combination of a number of radial basis functions, or as given by [Snyman & Wilke, 2017],

$$f(\mathbf{x}) \approx \sum_{j=1}^P w_j \phi_j(\mathbf{x}, \mathbf{x}_c^j) = \bar{f}(\mathbf{x}). \quad (\text{F1})$$

Radial basis functions,  $\phi_j$ , are formed considering the distance between the location of centre of the function  $\mathbf{x}_c^j$ , and the distance of some point from the centre of the function  $\mathbf{x}$ . These functions are then multiplied by a weighting,  $w$ . These weightings will need to be solved for in order to either meet all the training data exactly, or if fewer radial basis functions are used than data points in the training data, the least squares fit for all the points.

The radial basis function used was the Gaussian function, so the basis function will take the form

$$\phi_j(\mathbf{x}, \mathbf{x}_c^j) = \phi_j(r_j(\mathbf{x})) = e^{-\frac{1}{\epsilon} r_j(\mathbf{x})^2}, \quad (\text{F2})$$

with

$$r_j(\mathbf{x}) = \|\mathbf{x} - \mathbf{x}_c^j\|. \quad (\text{F3})$$

Here,  $\epsilon$  is known as the shape parameter which will need to be determined to produce a smooth and accurate surrogate model.

To this end, the RBF surrogate model in fact produces an interpolation of all the data points in the database. This interpolation is what provides the approximation to the objective function, and as more data points are added, the better the interpolation and approximation can be.

## APPENDIX G: INCLUSION OF SURFACE PROFILE IN DIRECT OPTIMISATION

To test the effect of the surface profile on convergence speed, several random starting points were chosen and ran for 50 objective function evaluations. The errors for each starting point were recorded, and made relative to the initial error. The average of these relative errors are shown in Figures G1, G2, and G3.

As can be seen in Figure G3, there is no conclusive trend for the  $\sigma$ - $\varepsilon_p$  curve error compared to the order of magnitude decreases found in Figure 28. The only noticeable trend is in Figure G2, where the inclusion of the surface profile does result in a performance increase when optimising for the surface profile. However, this is not surprising as the objective function now explicitly optimises the surface profile as well.

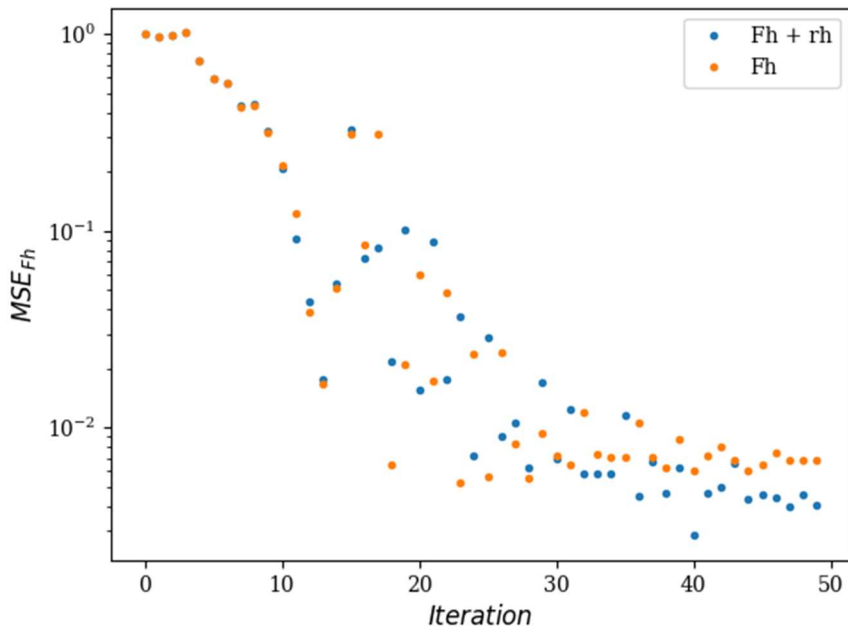


**Figure G1** Average relative MSE for F-h curve

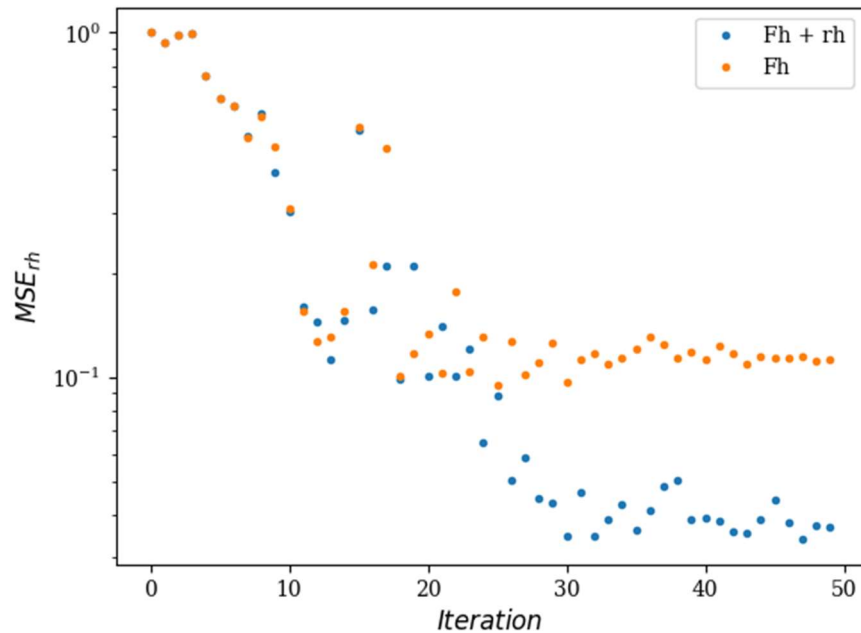


**Figure G2** Average relative MSE for surface profile

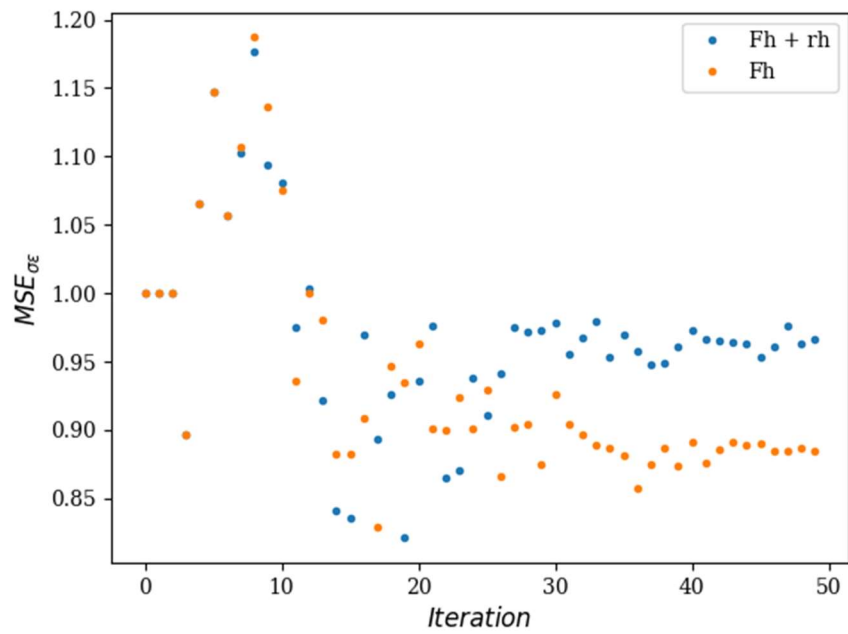


**Figure G3** Average relative MSE for  $\sigma\text{-}\epsilon_p$  curve

## APPENDIX H: PLASTIC STRAIN DISTRIBUTIONS

61/244:PE  
Time:0.610000  
Entity:PE  
+DispF:1.000000  
max: 6.62e-001  
min: -7.82e-005

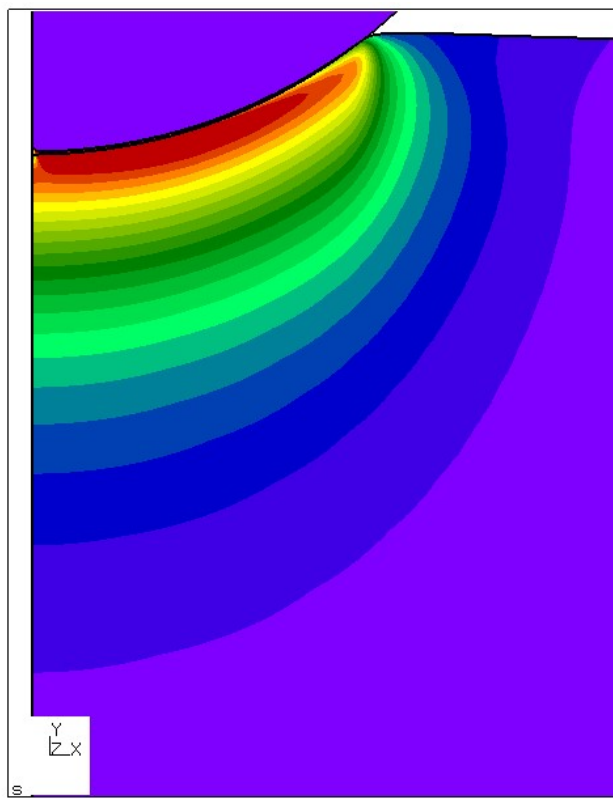
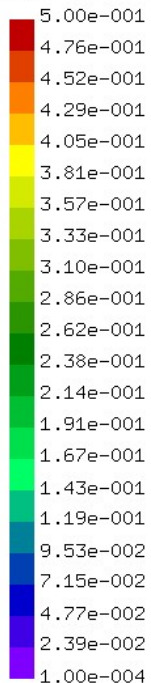


**Figure H1** Plastic strain distribution in target material

61/244:PE  
Time:0.610000  
Entity:PE  
+DispF:1.000000  
max: 6.17e-001  
min: -9.22e-005

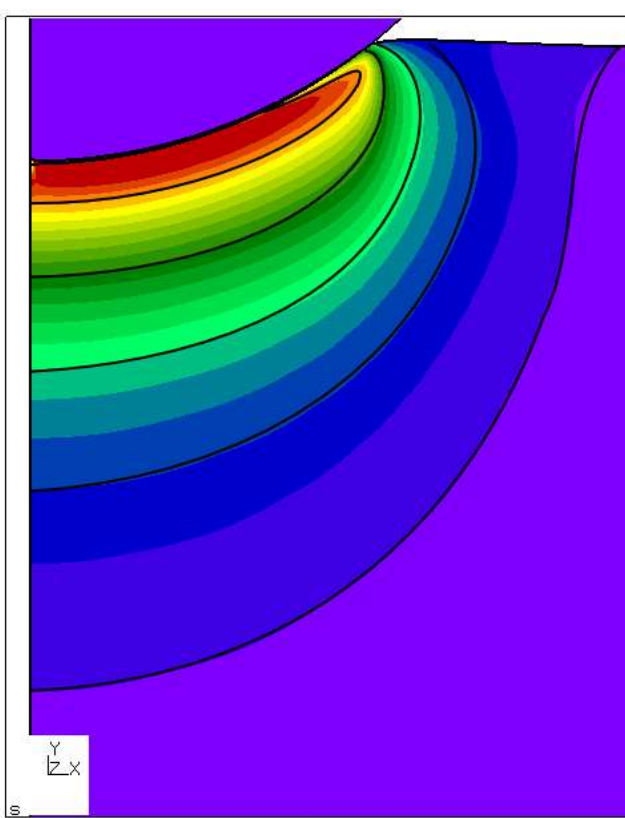
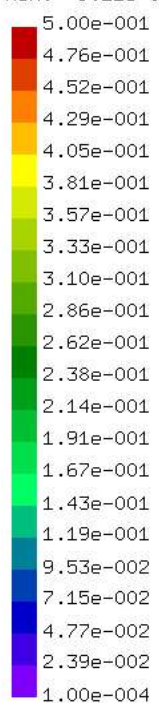


**Figure H2** Plastic strain distribution in worst-fit material with target material contours